UNIVERSITY OF CALIFORNIA, SAN DIEGO

Communication and Coexistence: Engineering Tools for Synthetic Microbial Ecosystems

A dissertation submitted in partial satisfaction of the requirements for the degree
Doctor of Philosophy

in

Bioengineering

by

Spencer R. Scott

Committee in Charge:

Professor Jeff Hasty, Chair
Professor Gurol Süel
Professor Kit Pogliano
Professor Yingxiao Wang
Professor Kun Zhang

2016

The dissertation of Spencer R. Scott is approved, and it is acceptable in quality and form for publication on microfilm and electronically:

_____

_____

_____

_____

_____
Chair

University of California, San Diego

2016

DEDICATION

"And because all things have contributed to your advancement, you should include all things in your gratitude." -Ralph Waldo Emerson

EPIGRAPH

What I cannot create, I do not understand.

Richard Feynman

TABLE OF CONTENTS

LIST OF ABBREVIATIONS

A.U. . . . . arbitrary units

bp . . . . . base pair

DNA . . . . . deoxyribonucleic acid

E. coli . . . . . *Escherichia coli*

Eq. . . . . equation

fig. . . . . figure

GFP . . . . . green fluorescent protein

QS . . . . . quorum sensing

AUC . . . . . area under curve

hrs. . . . . hours

kb . . . . . kilobase

LB . . . . . lysogeny broth

OD . . . . . optical density

ODE . . . . . ordinary differential equation

PCR . . . . . polymerase chain reaction

PDMS . . . . . poly(dimethylsiloxane)

UV . . . . . ultraviolet

CFP . . . . . cyan fluorescent protein

%w/v . . . . . percent weight per volume (concentration)

LIST OF FIGURES

LIST OF TABLES

LIST OF SUPPLEMENTARY FILES

Supplementary Video 1. Timelapse fluorescence microscopy of oscillatory lysis (LuxI-LAA) cells.

Supplementary Video 2. Timelapse fluorescence microscopy of constant lysis(untagged LuxI) cells.

Supplementary Video 3. Timelapse fluorescence microscopy of non-lysis Rpa-GFP and non-lysis Lux-CFP cells in a co-culture.

Supplementary Video 4. Timelapse fluorescence microscopy of lysis Rpa-GFP and lysis Lux-CFP cells in a co-culture.

Supplementary Video 5. Timelapse agent-based simulation of two lysis strains both in the oscillatory regime.

Supplementary Video 6. Timelapse agent-based simulation of two lysis strains one in the oscillatory regime and the other in the constant lysis regime.

ACKNOWLEDGEMENTS

I'm so overwhelmed by the amount of support I've received over the past four years, and so filled with gratitude for everyone that helped me along the way. First and foremost, I want to thank my parents for their unconditional love, unwavering encouragement, and unbeatable hospitality. I would be nowhere without them, and I can't imagine a more pleasant way to have spent my grad years than living with them and getting to experience life with them as an adult and their friend. I need to thank my siblings and friends, who across cities and states were my lifeline and emotional support system. I knew I could always turn to them for rejuvenation and camaraderie. With their smiles, hugs, and laughter I could, again, tap into the source of vitality, and continue on my journey happily. They absorbed my complaints, and reassured my soul. I can't thank them enough. My labmates - who were all much more than just co-workers - I'd like to thank for bringing liveliness to my days in the lab, for dancing with me in PPE, for laughing with me or at me or around me. They made lab-work so much more fun that it properly should be, and there's no one I'd rather have lunchtime intellectual pontifications with - from the academic to the absurd - in the whole wide world. I can't believe how lucky I am to have worked with such amazing people day in and day out, how fortune I am to have learned from them, and how grateful I am to have shared knowledge with them. I will miss these early mornings, sleepy afternoons, and late evenings in the lab with them all for the rest of my life. Last but not least, I have to thank my advisor Jeff Hasty for believing in me enough to give me plenty of space to prove myself. Not many other advisors would have given me so much trust and freedom, which ultimately allowed me to fully express my creativity through science. His own creativity unlocked many new potentials in my research and pushed me to see and connect with the bigger picture. Without his guidance I would have merely been - as Newton put it - "a boy playing on the sea-shore."

Chapter 2 contains material originally published as Scott, Spencer R., and Hasty,

Jeff ***ACS Synthetic Biology*** (2016): Quorum Sensing Communication Modules for Microbial Consortia. Copyright permission to republish here was granted by ACS publishing group. The dissertation author was the primary investigator and author on this paper.

Chapter 4 contains material being prepared for submission as Competitive Species Stably Co-Cultured in a Synthetic Microbial Ecosystem Through Orthogonal Self-Lysis. Scott, Spencer R., Din, M. Omar, Bittihn, Philip, Xiong, Liyang, and Hasty, Jeff. The dissertation author was the primary investigator and author on this paper.

VITA

2012	Bachelor of Science in Bioengineering University of California, Berkeley
2016	Doctor of Philosophy in Bioengineering University of California, San Diego

PUBLICATIONS

Peer Reviewed Journal Articles

Quorum Sensing Communication Modules for Microbial Consortia. Scott, Spencer R., and Hasty, Jeff ***ACS Synthetic Biology*** (2016)

Quorum Sensing Controlled Self-Lysis: Tools for Maintaining Competitive Species in a Synthetic Microbial Ecosystem. Scott, Spencer R., Din, M. Omar, Bittihn, Philip, Xiong, Liyang, and Hasty, Jeff ***Nature*** (being prepared for submission)

FIELDS OF STUDY

Major Field: Bioengineering (Synthetic Biology)

Studies in Biological Dynamics
Professor Jeff Hasty

ABSTRACT OF THE DISSERTATION

Communication and Coexistence: Engineering Tools for Synthetic Microbial Ecosystems

by

Spencer R. Scott

Doctor of Philosophy in Bioengineering

University of California, San Diego, 2016

Professor Jeff Hasty, Chair

The power of a single engineered organism is limited by its capacity for genetic modification. In order to circumvent the constraints of any singular microbe, a new frontier in synthetic biology is emerging: synthetic ecology, or the engineering of microbial consortia. In this thesis, we focus on engineering tools to facilitate communication and coexistence of microbial species in a synthetic ecosystem. Engineered microbial consortia are already being used to solve problems of waste recycling (Fulget et al., 1999), industrial fermentation (Chen, 2011; Patle and Lal, 2007), bioremediation (Dejonghe et al., 2003), and human health (Petrof et al., 2013; Khoruts et al., 2010; Shahinas et al., 2012), and we believe our tools will continue to further these advances. In Chapter One, I introduce the history and importance of synthetic biology and how engineering microbial ecosystems became the "second wave" of synthetic biology. In Chapter Two, I discuss the quorum sensing communication systems I developed in an effort to allow for complex social behavior across different members of a community. In Chapter Three, I

discuss several applications utilizing the myriad of described quorum sensing systems. In Chapter Four, I discuss a method to stably co-culture two metabolically competitive species using a recently developed population control circuit (Din et al., 2016) in conjunction with my novel quorum sensing systems. We posit that such engineered microbial communities will outpace monocultures in their ability to perform complicated tasks, and these chapters combine to enumerate the tools we've created to accelerate this emerging effort.

Chapter 1

Introduction

Personal Perspective

I started college as a Civil Engineer with the desire to become a sustainable or "green" architect. I bring this up because I believe my journey from architect to synthetic biologist stemmed from the same desire: to understand human's place within, and not apart from, Nature. And I believe this same desire is why so many young scientists are gravitating toward this field.

I absolutely love nature, but there seems to be a prevailing suspicion that to love nature inherently means to hate or distrust human activity. I, however, love human creation with the same passion that I love nature. And, truly, they are one in the same. Humans are no more apart from nature as chimpanzees or Mycoplasma are. The chasm of separateness exists only in our minds.

To see the hexagons of a beehive as miraculous but the structure of a city as a scar upon Earth, is to have lost hope in human creation. It is to believe that humans are ultimately destructive. While I don't think humans have perfected the art of creating without consequence; I often catch glimpses of promise. The hope of seeing humans as as a harmonious and miraculous part of an ecosystem, and the hope that we can see humans are ultimately creative.

This belief in human creativity within the bounds of ecological sustainability started me in "green" architecture but was eventually the reason I changed majors to Bioengineering. In college, I became enamored with biomimicry because it fascinated me that something so unassuming as a butterfly wing could hide a secret as phenomenal as structural color. It blew me away that our most sophisticated new tech was being informed by nature: things like the antimicrobial properties of shark skin, the water-repellant nature of a lotus leaf, or the magic grip of a gecko foot.

To me, the emergence of bio-informed design signaled the awakening of the human mind to Nature's calm ingenuity. It seemed there was so much to learn from what millions of years of evolution had to teach, and as Richard Feynman once said, "I cannot understand what I cannot build."

So, I sought to engineer biology to better understand it, and that's when I decided on the field of synthetic biology, and I presume many in the field have similar motivations. We are fascinated by the power of biology, the intricacies of nanomachines we call proteins, and the capacity of nanofactories we call microbes. We hope that by tinkering with the insides of these machines we can potentially build a sustainable future so that when we look at a city, we see human potential, not human destruction. So that new inventions bring excitement of possibilities and not a yearning for the past.

The Purpose of Synthetic Biology

Since the first genetic toggle switch was created (Gardner et al., 2000), synthetic biology has sought to understand life by engineering it from the bottom-up. This "investigation by re-creation" quickly expanded synthetic biology's toolkit to include a panoply of logic gates, filters, switches, sensors, and oscillators (Tamsir et al., 2011; Elowitz and Leibler, 2000; Gardner et al., 2000; Stricker et al., 2008; Tabor et al., 2009). Eventually, as the development of synthetic biology continued, certain biological standards were created (Canton et al., 2008) to turn this field from a disjointed art into an engineering discipline. The philosophy behind modular genetic parts (Voigt, 2006)

would form the basis of future genetic tinkering.

Researchers eventually moved beyond re-creating and mimicking gene networks to focus on real-world applications like engineering bacteria capable of invading cancer cells (Anderson et al., 2006), modifying yeast cells to produce a potent antimalarial precursor drug that could drastically expand its commercial availability (Paddon et al., 2013), or tackling the energy crisis by engineering bacteria to produce biodiesel hydrocarbons (Steen et al., 2010). While synthetic biology will continue to be a useful tool for deconstructing and understanding natural phenomena; much of the future of synthetic biology will be focused on putting these nanofacotires to work in real-world applications.

And although monoclonal synthetic biology has led to increased efficiency in the production of important industrial chemicals and “high value” products (Khalil and Collins, 2010; Ro et al., 2006; McDaniel and Weiss, 2005), the production capacity of a single organism is limited by metabolic load and byproduct toxicity. As a way to overcome this constraint, recent evidence suggests that engineered communities (synthetic microbial ecosystems) will be able to pick up where monocultures have left off (McMahon et al., 2007) and usher in the "second wave of synthetic biology" (Purnick and Weiss, 2009).

The Promise of Synthetic Microbial Ecosystems

One of the more convincing arguments for synthetic microbial communities is the advantage of a syntrophic artificial consortia whereby one species can metabolize an otherwise toxic byproduct the other species produces (Figure 1.1). For example, (Zhou et al., 2015), used *S. cerevisiae* to limit the toxic byproducts of an engineered *E. coli* attempting to produce anti-cancer therapeutic precursors. Other groups have accomplished similar feats of mutualism using two related *Geobacter* species capable of electron sharing (Summers et al., 2010), and a consortia of *Methanococcus maripaludis* and *Desulfovibrio vulgaris* that were more metabolically productive together than they

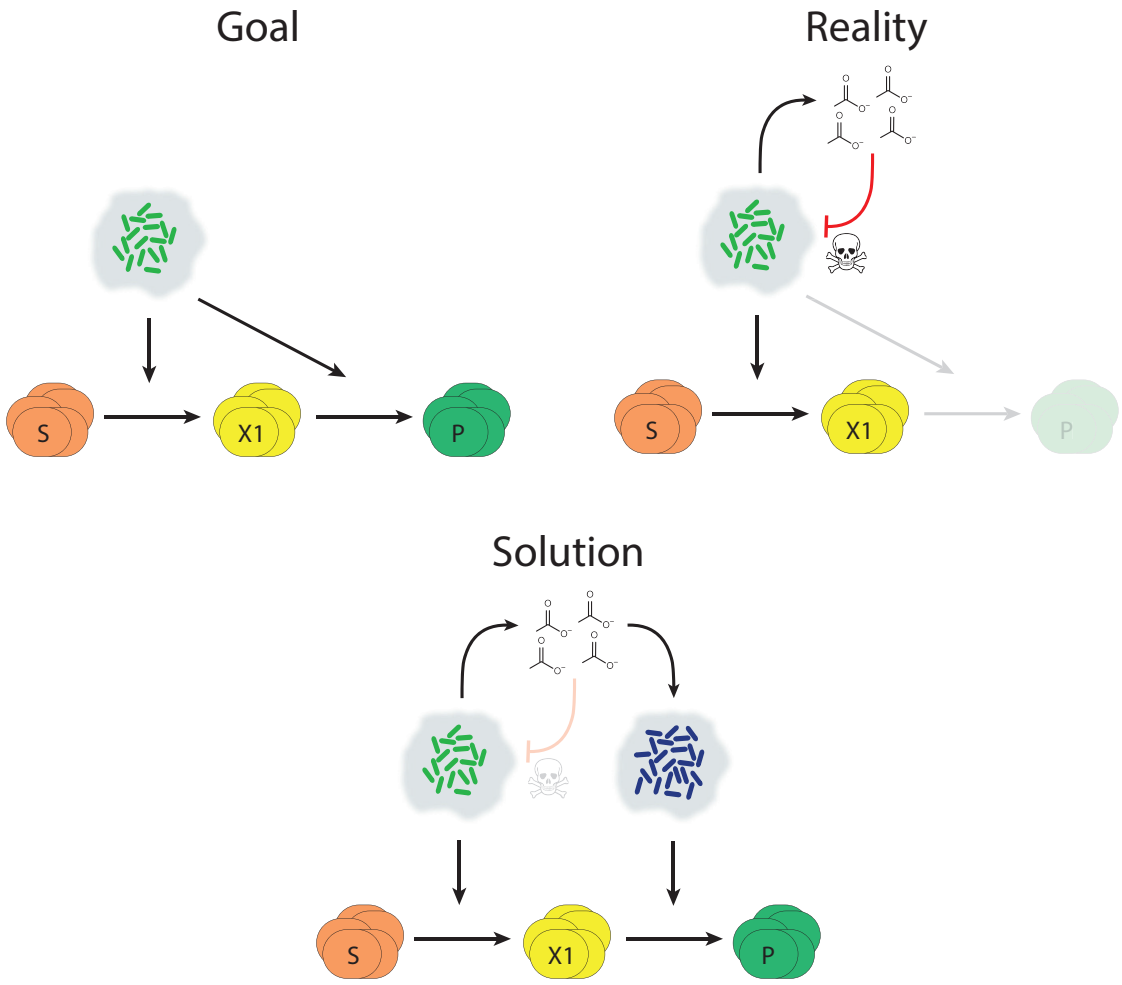

Figure 1.1: The Limitations of Monocultures. Many goals in synthetic biology are based on based on engineering a metabolic network to convert a feedstock substrate (S), through one or more intermediates (X) to a final product chemical (P). However, reality often presents challenges in the form of diauxic growth, low yields, or byproduct toxicity as is there case here, making efficient product production unfeasible. One solution, as previous groups have demonstrated, is to introduce a second species that compliments the deficiencies of the first species. This is an example of a synthetic microbial ecosystem. Figure inspired by (Brenner et al., 2008).

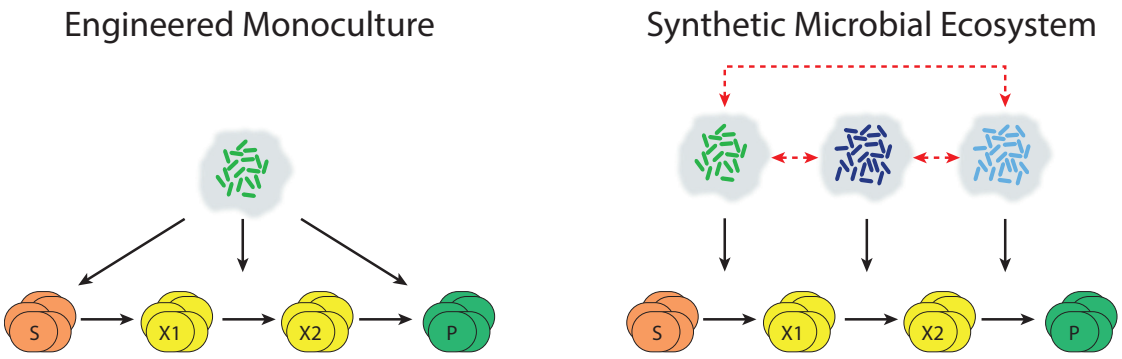

Figure 1.2: From Engineered Monoculture to Synthetic Microbial Ecosystem. On the left is a schematic of an engineered "superbug" that is tasked with multiple metabolic steps that could potentially dampen its fitness, slow its growth rate, or produce intermediates that are directly toxic. On the right is a schematic for the concept of specializaiton and load distribution via a synthetic microbial ecosystem that divides tasks amongst members of the community for optimal performance. Figure inspired by (Ford and Silver, 2015)

were individually (Hillesland and Stahl, 2010). Together, these studies inform our understanding of how specialization of organisms will offer a solution to many problems associated with conventional metabolic engineering.

Furthermore, the defining goal of an engineered “superbug” capable of high-yield production (Brenner and Arnold, 2011) is discordant with established ecological theory that the optimization of one trait occurs at the price of other necessary traits (Carlson and Taffs, 2010; Kneitel and Chase, 2004). It therefore makes less sense to engineer a single species that takes a substrate through multiple laborious metabolic steps to reach the final product, when a microbial community composed of specialized cells could accomplish the same metabolic steps with less stress on each individual and therefore, a greater potential to create the product at higher efficiencies (Figure 1.2).

While the promise of engineering microbial consortia is high, the tools available to build and control such communities are still few and far between. In an effort to address this problem we identified two general mechanisms that need to be addressed in order to successfully engineering such ecosystems: communication and coexistence.

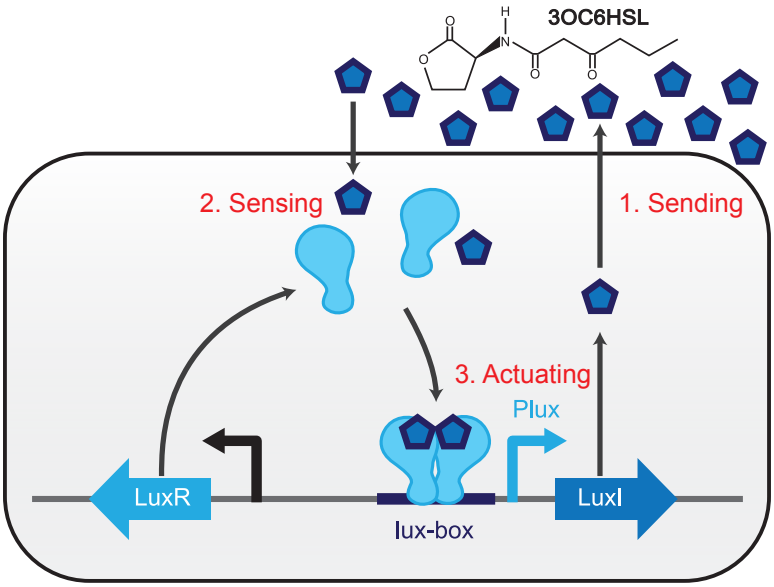

Figure 1.3: Wild-type Quorum Sensing in *Vibrio fischeri*. (1.) Sending: Basal expression of LuxI allows slow accumulation and production of signal molecule, 3OC6HSL. (2.) Sensing: At high cell-densities this molecule accumulates above a threshold concentration at which point it can bind and activate LuxR. (3.) Actuating: AHL-bound LuxR is then capable of binding to the lux-box upstream of the Plux promoter. It then recruits sigma factor binding and transcriptional up-regulation of *luxI* and other proteins regulated by the lux system. Since AHL-bound LuxR increases production of LuxI, the system as a whole is a positive feedback mechanism.

Communication

Quorum Sensing

Communication as a means of regulation is essential for cooperative behavior in microbial consortia. Quorum sensing (QS) is a common mechanism used by bacteria to sense local cell density in order to coordinate gene expression and affect differential behavior (Ng and Bassler, 2009), and can be coopted to accomplish general communication between and amongst members of a community.

Quorum sensing communication is accomplished through a three stage process of sending, sensing, and actuating (Figure 1.3). The sending process consists of synthesizing a small molecule, which in the case of *Vibrio fischeri* is a homoserine-lactone (HSL) called 3-oxo-C6 HSL (C6HSL) produced by the LuxI enzyme. As individual

members of the culture contribute to the aggregate concentration of C6HSL, the concentration eventually reaches the quorum threshold at which point HSL binding to the constantly present receptor, LuxR, becomes increasingly favorable. When LuxR binds its cognate HSL it becomes active and its DNA-binding domain attaches to the Plux promoter and drives transcription of lux-regulated genes (Ng and Bassler, 2009).

Although this is only one major type of quorum sensing (Waters and Bassler, 2005), we focus on the LuxR/LuxI-type systems mediated by homoserine lactone (HSL) ligands because of their simplicity and large natural diversity (Ng and Bassler, 2009; Miller and Bassler, 2001; Davis et al., 2015). Furthermore, many naturally occurring Lux-like quorum sensing systems have already been identified (Figure 1.4), and this base-level characterization becomes useful when trying to engineer communication systems for microbial consortia.

Because of the richness in availability and diversity of lux-like quorum sensing systems, we chose to engineer communication systems based on these modular systems. We began by deconvoluting the possible ways in which two strains could theoretically communicate using quorum sensing systems alone. Expanding from monocultures to just two-strain ecosystems, a large set of possibilities emerge.

If a strain does not send a signal it is characterized as having no communication (None). If a strain receives a signal it itself sends, it has intra-communication (Intra). If a strain sends a signal that it does not receive itself, it has inter-communication (Inter), if it sends a signal that is received by both it and another member of the community it has both Intra and Inter-communication (Intra/Inter). Since both strains could be capable of such a dynamic, there are a resulting sixteen different basic communication motifs possible (Figure 1.5). Interestingly, there are certain combinations that, by nature, require levels of signal orthogonality (or the absence of signal crosstalk; see Figure 2.1), a reality not so easily achieved with real quorum sensing systems which we will discuss in Chapter 2 and Chapter 4.

However, it also becomes clear that a small set of quorum sensing systems could unlock many possibilities in both monoculture and microbial consortia dynamics. In

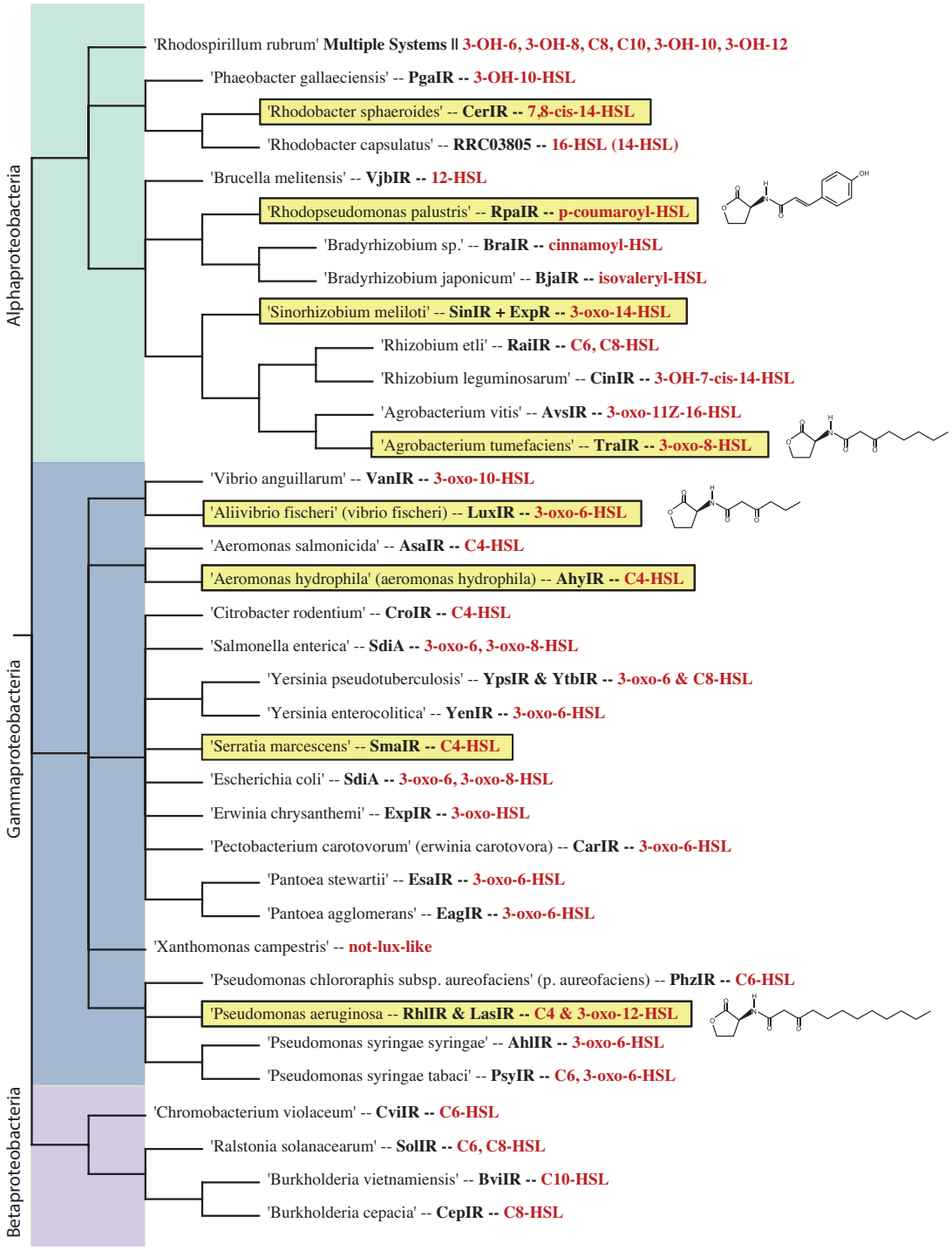

Figure 1.4: Evolutionary Tree of Selected Lux-like QS Systems. Systems selected for initial analysis are highlighted in yellow. Each system's HSL is written in red; the chemical structure of the four HSL's particular to the systems characterized in this study are shown on the far right. Potential systems were chosen based on evolutionary distance, ligand uniqueness, and available information in the literature on their potential for recombinant expression

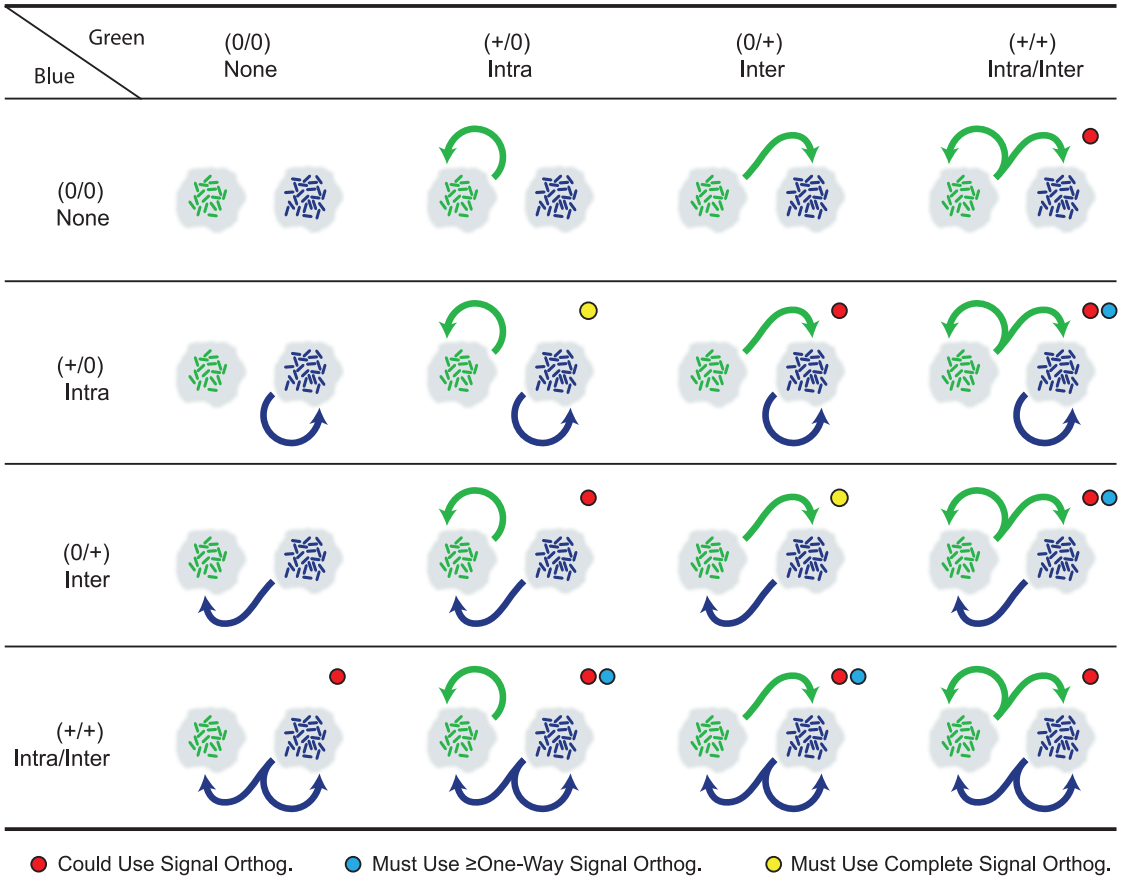

Figure 1.5: Possible Communication Motifs of a Two-Species Synthetic Microbial Ecosystem. There are 16 basic quorum-sensing motifs possible in a two-strain consortia, with each strain capable of no, intra-, inter-, or both intra- and inter-communication. Green arrows represent a quorum-sensing signal produced by the green strain, blue arrows represent a quorum-sensing signal produced by the blue strain. Red dots next to a particular motif indicate the possibility for signal orthogonal QS systems to be used. Blue dots next to a particular motif indicate the need for two QS systems to have at least one-way signal orthogonality. Yellow dots indicate the need for complete, both-way signal orthogonality in order to achieve that particular motif.

Chapter 3 we discuss several potential applications of our characterized quorum sensing systems, and then transition into the specific application of engineering coexistence.

Coexistence

The second but ultimately most important aspect of building synthetic microbial consortia is determining how they will coexist. Ecologically or metabolically speaking there are six major ways in which two species can interact (Figure 1.6) (Großkopf and Soyer, 2014). The trivial case of no interaction is highly unlikely, but if the two strains were co-cultured they would still compete for space and the faster growing strain would take over (this will be discussed in depth in Chapter 4). Of the more likely instances, commensalism, amensalism, cooperation, predation, and competition, only cooperation or "mutualism" will most readily result in a stable co-culture (Faust and Raes, 2012; Großkopf and Soyer, 2014; De Roy et al., 2014). The exception being a predator-prey situation where the predator depends on the prey as its food source, thereby allowing oscillatory coexistence (Balagaddé et al., 2008; Kerr et al., 2002). Nevertheless, it is still rare that two randomly selected strains will be naturally cooperative, or their coexistence be mutually beneficial. More likely, as has been shown to be the case (Foster and Bell, 2012; Freilich et al., 2011), the engineering of microbial consortia will face a lot of naturally competitive species and it will be up to researchers to engineer new ways to co-culture such strains. In Chapter 4, we describe a system by which we accomplish this goal of stably co-culturing two metabolically competitive strains.

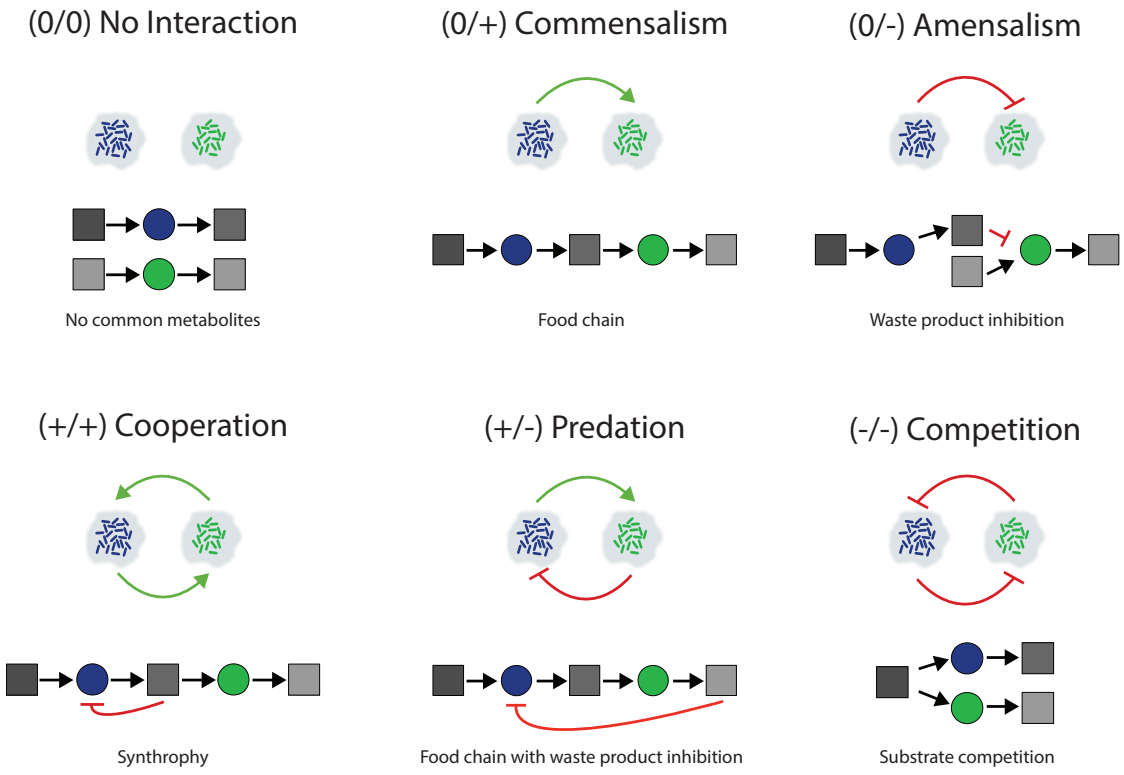

Figure 1.6: The Basic Coexistence Motifs of a Two-Species Synthetic Microbial Ecosystem. On top is the ecological representation of interaction, and on bottom is the matching metabolic interaction. Grey boxes represent different food sources and metabolic products. Blue and green circles represent the blue and green strains, respectively. Stimulating, or helpful, interactions and their direction are denoted with green arrows, while inhibitory, or harmful, interactions and their direction are denoted with red arrows. Figure adapted from (Großkopf and Soyer, 2014)

Chapter 2

Characterizing Communication Modules for Microbial Consortia

Introduction

Monoclonal synthetic biology has led to increased efficiency in the production of important industrial chemicals and "high value" products (Khalil and Collins, 2010; Ro et al., 2006; McDaniel and Weiss, 2005). However, the production capacity of a single organism is limited by metabolic load and byproduct toxicity, which are both difficult to address with intracellular genetic optimization (Dueber et al., 2009; Kizer et al., 2008; Zhu et al., 2002; Barbirato et al., 1996). Furthermore, the defining goal of an engineered "superbug" capable of high-yield production (Brenner and Arnold, 2011) is discordant with established ecological theory that the optimization of one trait occurs at the price of other necessary traits (Carlson and Taffs, 2010; Kneitel and Chase, 2004). Due to recent evidence that robust communities will out-perform optimized monocultures (McMahon et al., 2007), a new frontier in synthetic biology is emerging: synthetic ecology, or the engineering of microbial consortia (Brenner et al., 2008; Pandhal and Noirel, 2014; De Roy et al., 2014; Dunham, 2007; Mee et al., 2014).

Engineered microbial communities have already demonstrated that the limita-

tions imposed by metabolic load can be addressed through distribution and specialization across various members of a community (Arai et al., 2007; Vinuselvi and Lee, 2012). This allows consortia to produce higher yields (Bernstein et al., 2012; Minty et al., 2013) and to optimally respond to diauxic growth (Eiteman et al., 2008) or harsh environmental fluctuations (Burmolle et al., 2006; LaPara et al., 2002; Fay, 1992). Importantly, the engineering of microbial consortia will also facilitate a systematic understanding of native communities that are of increasing importance in the context of the human microbiome and significant environmental challenges (Shou et al., 2007; Balagaddé et al., 2008; West et al., 2006).

Regulatory processes are essential for cooperative behavior in microbial consortia. Quorum sensing (QS) is a common mechanism used by bacteria to sense local cell density in order to coordinate gene expression and affect differential behavior (Ng and Bassler, 2009). Species capable of such sensing harbor regulator proteins that, when bound to a particular ligand, modulate transcription from various QS promoters (Ng and Bassler, 2009). Although there are several different QS mechanisms (Waters and Bassler, 2005), the LuxR/LuxI-type systems mediated by homoserine lactone (HSL) ligands are the most promising due to their simplicity and large natural diversity (Ng and Bassler, 2009; Miller and Bassler, 2001; Davis et al., 2015). QS is a reliable and well-characterized tool synthetic biologists have used for a variety of applications including triggering biofilm formation (Hong et al., 2012; Kobayashi et al., 2004), constructing synchronized oscillators (Prindle et al., 2014; Danino et al., 2010), generating patterns (Basu et al., 2005; Payne et al., 2013), sensing pathogens (Saeidi et al., 2011), and developing synthetic ecosystems (Balagaddé et al., 2008; Brenner et al., 2007). Furthermore, QS has proved to be a powerful tool for metabolic engineering, by allowing timed production of chemicals to commence at optimal cell-densities (Brockman and Prather, 2015; Srimani and You, 2014; Pai et al., 2012; Tsao et al., 2010).

Taken collectively, these studies have established a foundation for the use of quorum sensing in microbial consortia. However, until recently (Wu et al., 2014), the cross-interactions between QS systems have received little attention. If multiple sys-

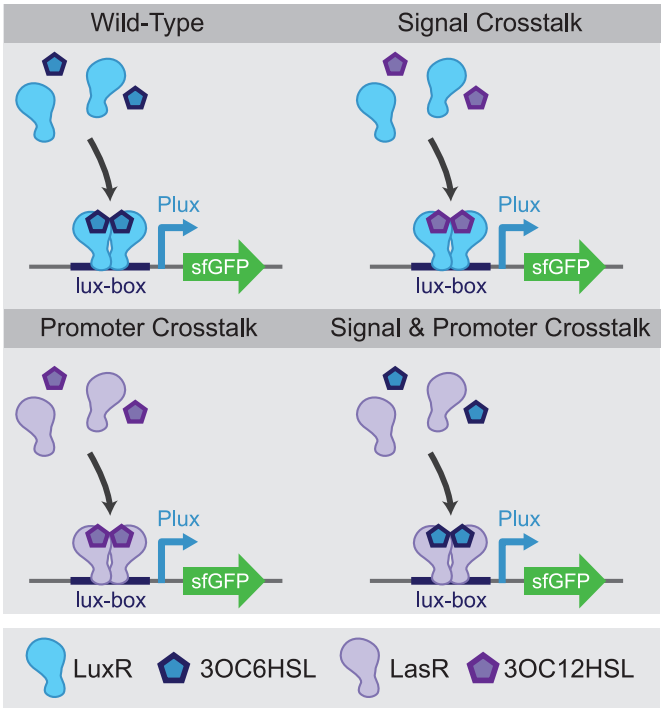

Figure 2.1: Potential Sources of Crosstalk Between Quorum Sensing Systems. Top left: R-protein (LuxR) binds its cognate ligand (3OC6HSL) to become active and drive transcription from the Plux promoter. Top right: Signal crosstalk occurs when the R-protein can become active through binding of an HSL other than its cognate ligand, such as LuxR binding 3OC12HSL, common to the las system. Bottom left: Promoter crosstalk occurs when the QS promoter of one system can be activated by the active R-protein of another system, such as Plux being activated by LasR bound to 3OC12HSL. Bottom right: Mixtures of both signal and promoter crosstalk can occur, allowing a R-protein from one system to bind an off-target ligand and activate a non-canonical promoter.

tems are to be used in the same environment, it is important to know how they will interact with one another. Two QS systems in the same population can harbor either signal crosstalk, promoter crosstalk, or a mixture of both (Figure 2.1). Signal crosstalk occurs when a receptor can bind a non-canonical HSL, such as LuxR binding 3-oxo-C12-HSL (3OC12) which is native to the las system. Promoter crosstalk occurs when an activated receptor can bind a non-canonical promoter, demonstrated by an activated LasR being capable of driving transcription off the Plux promoter. Covering all possible combinations reveals that a mixture of these two crosstalks is possible, whereby a receptor is activated by a non-canonical HSL and then activates a non-canonical promoter (Figure 2.1).

Through promoter and protein engineering, the rpa and tra quorum sensing systems were modified to allow functionality in *E. coli*, adding two more systems to the previously characterized lux and las systems. To the best of our knowledge the rpa system has never been described in *E. coli* before, and the tra system, although well-characterized in *A. tumefaciens* and *in vitro*, (Zhu and Winans, 1999; Fuqua and Winans, 1996; White and Winans, 2007) has otherwise been previously shown to exhibit poor activity in whole E. coli cells (Zhu and Winans, 1999). All possible cross-interactions between these systems' components were then tested to understand how they could be used in an engineered community.

Most systems exhibited varying levels of crosstalk, and while unexpected interference between components can cause a loss of circuit function (Brophy and Voigt, 2014; Wu et al., 2014), if the parts are well-characterized the crosstalk can be harnessed to create unique dynamical circuits. In other cases it can be advantageous to have communication systems that function orthogonally. For the purposes of this study, we defined orthogonality as such: system A is said to be "signal orthogonal" to system B if Receptor A cannot be activated by Signal B, "promoter orthogonal" to system B if Promoter A cannot be activated by an HSL-bound Receptor B, and "completely orthogonal" if both cases are true. Orthogonality can therefore only be defined under a given concentration range of the signal and also depends on the definition of "activated". We

considered a system activated if it exhibited a maximum fold-change greater than 2, or an Area Under the Curve (AUC) greater than 2% of the canonical AUC response, as defined for Figure 2.5.

Several groups have pointed out the utility of complete orthogonality (Chuang, 2012) and even used different classes of QS systems (Marchand and Collins, 2013; Quan et al., 2016; Shong and Collins, 2013) in concert with Lux-like QS systems to accomplish such orthogonality. Here we demonstrate that different combinations of our Lux-like QS systems can achieve signal, promoter, and complete orthogonality. By characterizing the varying degrees of cross-talk and orthogonality between all four systems and their components, we hope to facilitate the development of synthetic microbial communities with well-controlled functionality.

Results

Screening Lux-like QS Systems

Lux-like quorum sensing systems are widely dispersed throughout the proteobacteria phyla, each with a unique LuxR-like receptor and HSL homolog (Gray and Garey, 2001; Waters and Bassler, 2005). Taking advantage of the natural diversity of these receptors and ligands, several systems were chosen based on their "evolutionary distance" and ligand uniqueness (Fuqua et al., 1996; Gray and Garey, 2001) (see Figure 1.6). The systems that were chosen include the lux system from *Vibrio fischeri* with ligand 3-oxo-C6-HSL (3OC6) (Gray and Garey, 2001), the las and rhl system from *Pseduomonas aeruginosa* with ligand 3OC12 and C4-HSL respectively (Fuqua et al., 1996), the tra system from *Agrobacterium tumefaciens* with ligand 3-oxo-C8-HSL (3OC8) (White and Winans, 2007), the rpa system from *Rhodopseudomonas palustris* with ligand p-coumaroyl-HSL (pC) (Schaefer et al., 2008; Hirakawa et al., 2011), the ahy system from *Aeromonas hydrophilia* (Swift et al., 1997), the sma system from *Serratia marcescens* (Thomson et al., 2000), the cer system from *Rhodobacter sphaeroides* (Puskas et al.,

1997), and the exp system from *Sinorhizobium meliloti* (Charoenpanich et al., 2013).

To assure reliable gene expression, each LuxR-like protein from the selected systems was GFP tagged to gauge translational output. After all of the R-protein-fusions were shown to express well (Figure 2.2A), each R-protein was tested for native functionality by co-transforming it with a GFP reporter plasmid harboring its native promoter (see Table C.1 (Fuqua and Winans, 1996; Hirakawa et al., 2011; Garde et al., 2010; Slater et al., 2003; Karig and Weiss, 2005; Puskas et al., 1997; Charoenpanich et al., 2013)). Despite evidence of successful expression of R-proteins, none of the systems other than the extensively characterized lux and las systems showed GFP induction in the presence of its HSL ligand. Several possible points of failure were identified; for example, protein misfolding may impede proper ligand or DNA binding, or recruitment of *E. coli*'s sigma factor may necessitate a slightly different protein location/conformation than the system's native chassis. In order to address these issues, we rationally designed and tested new promoters and proteins.

Rational Design of QS Systems

Using the lux-system as a point of reference for a QS system that functions in *E. coli*, hybrid promoters, Ptra* and Prpa*, were created by replacing the lux-box in the commonly used PluxI promoter with the tra-box (White and Winans, 2007) and rpa-box (Hirakawa et al., 2011), respectively. This drastically improved the fold change of the rpa system from no-significant induction to nearly a 25x fold change in the presence of its cognate ligand (Figure 2.2B). The tra system was also improved from no significant induction, but its fold change was still rather low (Figure 2.2C). Observing protein alignment across several LuxR-homologs, it was noted TraR was missing a conserved tryptophan amino acid (Vannini et al., 2002), which in LuxR is known to be important for sigma factor recruitment (Fuqua and Greenberg, 2002). Engineered receptor TraR(W) was created by substituting a tryptophan into the correct amino acid position. When combined with the Ptra* promoter and the native signal, the fold change was dou-

bled compared to the wild-type TraR protein and hybrid Ptra* promoter (Figure 2.2C).

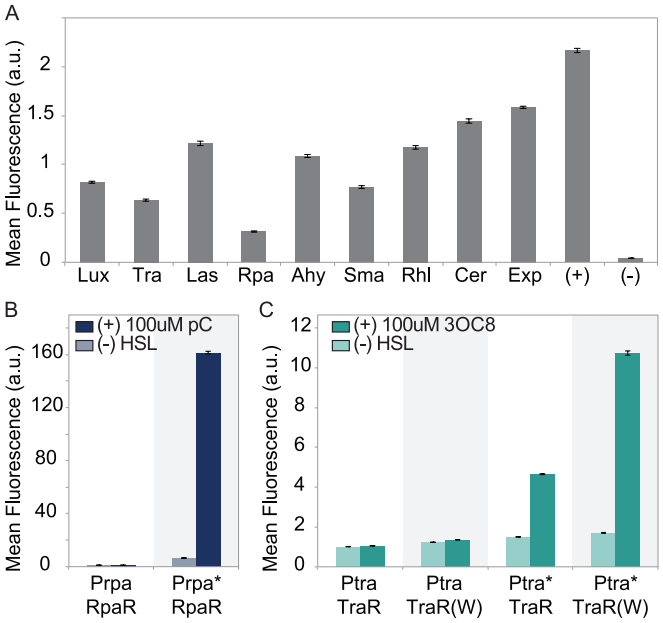

Figure 2.2: Engineering New QS Systems in *E. coli* (*A*) Mean fluorescence of GFP-LuxR-like protein fusions. Positive control is constiutively expressed GFP, and negative control is the *E. coli* strain with no GFP plasmid. (*B*) Wild-type rpa-promoter is non-functional in E.coli, however an engineered Plux-rpa promtoer functions well. (*C*) Wild type tra-promoter is also non-functional, but an engineered Plux-tra promoter shows significant fold-change in the presence of cognate ligand. Also, an engineered TraR with a point mutation to increase sigma factor binding increases fold change of the tra system. (*B*),(*C*) Mean values are normalized by lowest expression in each panel. Error bars represent S.E.M (n=3).

Quorum Sensing Circuit Multiplexing

In order to fully characterize the utility of these QS-responsive strains, a modular two plasmid system was constructed such that an actuator plasmid constitutively produced the LuxR-like protein, while a reporter plasmid harbored a single QS-promoter expressing sfGFP (Figure 2.4A). With the four functional systems (lux, tra, las, and rpa), all sixteen possible actuator/reporter two-plasmid strains were created. Each receptor protein, without any HSL ligand, has an inherent affinity for each promoter, giving each of these sixteen combinations a unique basal expression level or “leakiness” (Table 2.1),

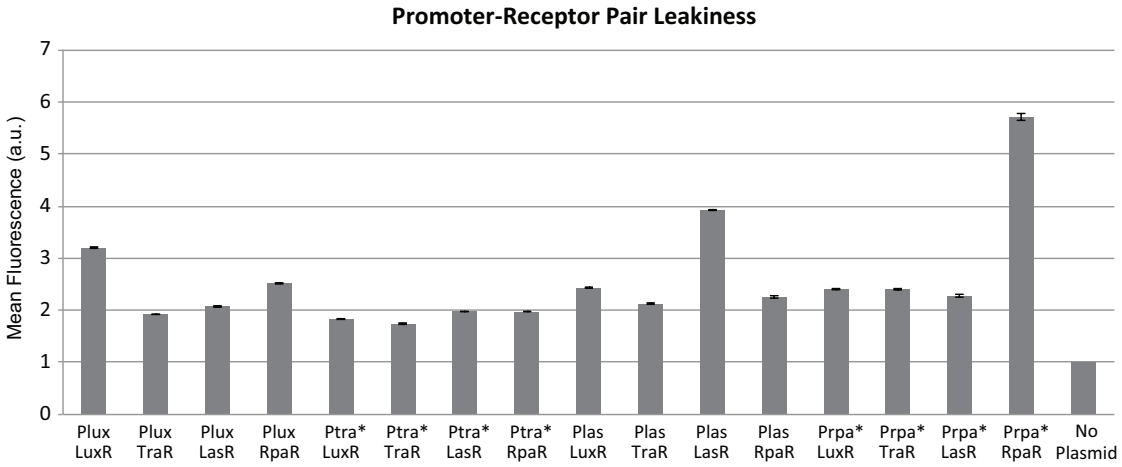

Figure 2.3: Promoter/Receptor Pairs Exhibit Differential Basal Expression Levels. Mean fluorescence of Receptor/Reporter two-plasmid systems in the absence of any HSL signal. All values are normalized by the auto-fluorescence of the same E. coli strain with no GFP plasmid. Error bars represent S.E.M (n=3).

defined as the GFP expression in the absence of any HSL ligand, normalized by the observed fluorescence of the same *E. coli* strain without a GFP plasmid (Figure 2.3). Leakiness can negatively affect genetic circuit functionality, or it can be harnessed to direct the rates of transient protein expression, making basal expression an important characteristic. Interestingly, the canonical R-protein and its respective promoter were seen to always harbor the highest leakiness for each promoter/receptor set. This finding suggests that if leakiness is an undesirable trait for a potential genetic circuit, a non-canonical yet functional R-protein could be used instead.

Each of these sixteen strains were exogenously subjected to a wide concentration range of the four characteristic HSLs, and the resulting GFP production after three hours of incubation was measured (Figure 2.4B). The concentration maximum (100uM) was limited by physiologically relevant numbers (Miller and Bassler, 2001), while the minimum (1E-10 or 1E-14M) by previously observed response thresholds (data not shown). Only promoter/receptor pairs that showed a 2-fold induction or more in the presence of at least one HSL were shown in Figure 2.4, for all combinations not shown it can be inferred they exhibited no significant response under any conditions. QS constructs

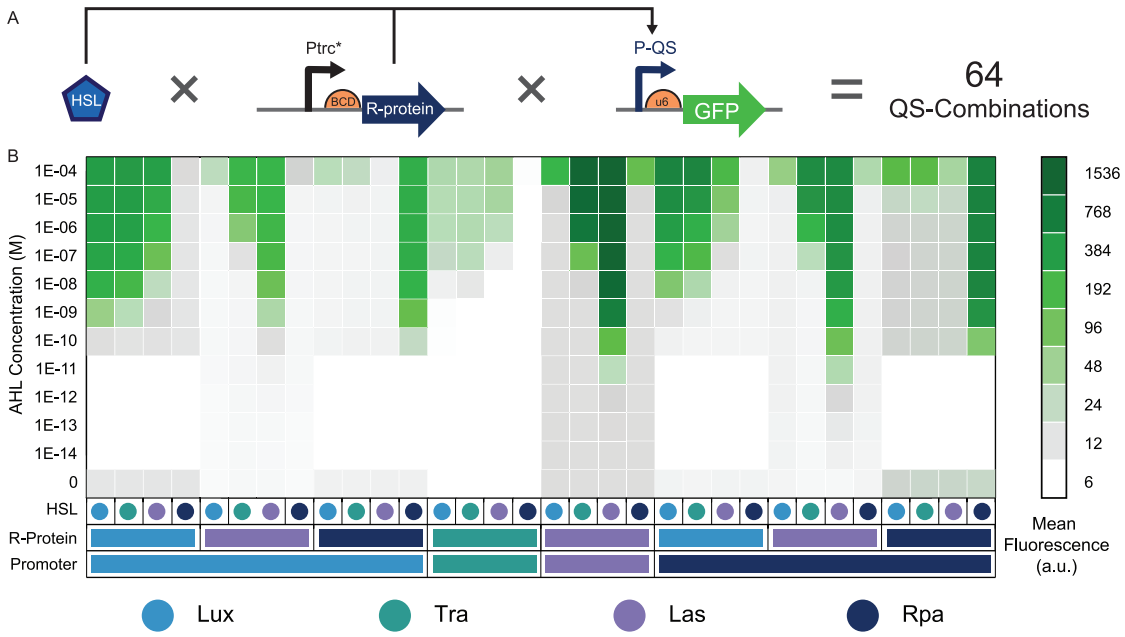

Figure 2.4: Dose-Response from Multiplexed Quorum Sensing Circuits (*A*) Genetic schematic of a single construct in the presence of a particular HSL ligand. With four R-proteins and four promoters there are 16 two-plasmid combinations each induced with four different HSLs giving 64 promoter/R-protein/HSL combinations measured at 8 ligand concentrations (or 12 for LasR). (*B*) Heat map showing GFP abundance for all QS combinations and HSL concentrations. Each column denotes a unique combination of signal (HSL), receptor (R-protein), and reporter (QS promoter), with rows denoting the concentration of ligand. Only Promoter/R-protein combinations that resulted in at least a 2-fold increase for one or more HSL are shown. Each value corresponds to the mean fluorescence value measured from a cell population normalized by the population's cell-density; all combinations and concentrations were done in triplicate.

are denoted by a three letter system where "L" refers to the lux system, "T" to the tra system, "A" to the las system, and "R" to the rpa system; the first letter denotes the promoter used, the second letter the R-protein used, and the third letter the HSL used (Plux+LasR+3OC8= "LRT"). This fully comprehensive assay elucidated all three potential crosstalk dynamics, as well as extensively characterized many new inducible genetic circuits. Each construct's relevant behavior was quantified by fitting its expression data to the typical dose-response function:

$$GFP = b + \frac{a-b}{1+10^{\log(EC50-X)*h}}$$

Where a is the maximum response, b is the basal expression, X is the concentration of ligand, and GFP is the response at that concentration. In order to assure meaningful fitted dose-response curves, only the QS pairs that showed significant activation before 100uM were analyzed. From this equation, four important attributes of each dose response curve were calculated: fold change, EC50, hill slope (h), and area under curve (AUC) or "activity area" (Yadav et al., 2014; Huang and Pang, 2012) (Table 2.1). Fold change is defined as the maximum observed expression divided by the basal expression in the absence of ligand (a/b). The EC50 is defined as the concentration of ligand that results in half-maximum activation of the QS construct. The hill slope is defined as the steepest slope along the dose response curve, and is indicative of how responsive the promoter/receptor pair is to the ligand. Lastly, the fitted curve was integrated using a trapezoidal function to calculate the area under the curve minus the area of the leakiness to give the activity area (Figure 2.5C). Generally, the Las system demonstrates the highest fold change and has a relatively low (strong) EC50, the Tra system has the lowest fold change and weakest EC50 but is also the least leaky. The Rpa system has the strongest EC50 and the highest leakiness, and the Lux system has mid-range values for all characteristics.

Fold change is a very important aspect of genetic circuits, and this multiplex assay allowed the identification of systems with a wide range of induction curves rang-

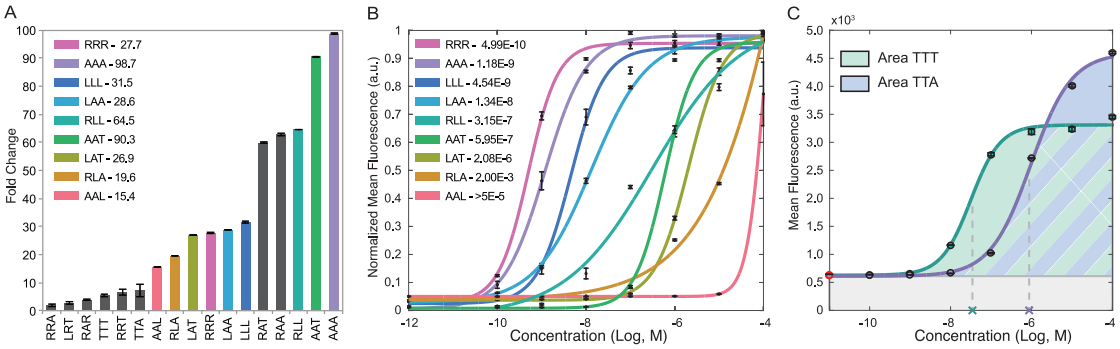

Figure 2.5: Activity Area of Dose-Response Curve as Performance Standard. (*A*) The maximum fold-change of a diverse subset of the QS constructs after 3 hours of induction. (*B*) Normalized dose-response curves of a subset of QS constructs that demonstrate a variety of EC50s. Each curve is normalized by its own maximum value, such that each curve converges to 1. (*C*) Fitted dose-response curves to the experimental data and their calculated activity areas. The red dot indicates the mean expression in the absence of HSL. Grey box under the curve represents the inherent leakiness of the circuit. Where the dotted lines meet the x-axis gives the EC50 value. Error bars indicate the standard error of the mean (n=3).

ing from 2-fold to almost 100-fold in batch culture after three hours of induction (Figure 2.5A). However, the use of fold change as a standard to compare QS circuit performance was obfuscated by unexpected expression dynamics. For example, TTA shows a greater fold change than the canonical TTT, yet is much less sensitive to the exogenous ligand with an EC50 almost two orders of magnitude higher (Figure 2.5C). This phenomena may be the result of different HSL stabilities, but is more likely due to the receptor having a slightly different conformation when bound to the off-target HSL, allowing it to bind tighter to the DNA or recruit the sigma factor more strongly. Such a unique crosstalk dynamic may have implications in natural systems that would benefit from a strong response to high levels of a foreign species. Fold change was further determined to be misleading because many systems showed steep increases in induction at 100uM, while at 10uM they still exhibited near-background expression (Figure 2.6). AAL, for instance, has a fold change of 15, yet its activity area is about 1% that of the canonical (AAA). The normalized activity area of 1% gives a much more accurate account of its relative performance than the normalized fold change (15% of the max

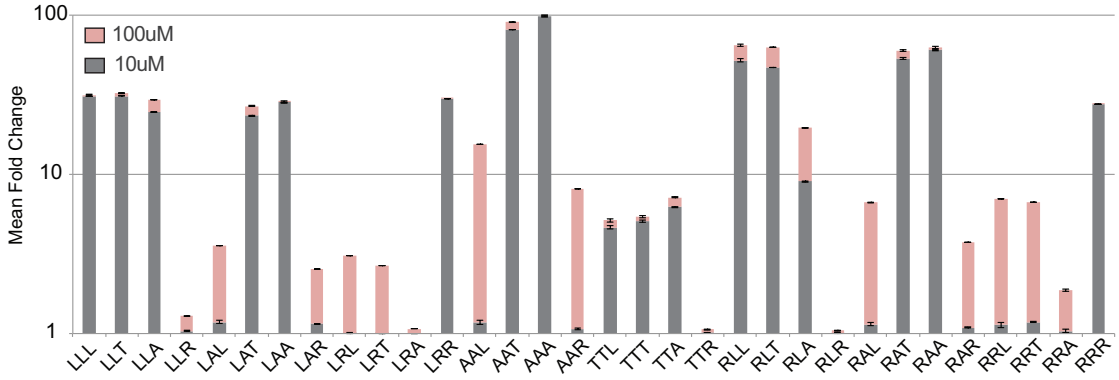

Figure 2.6: Large Increase in Expression at 100uM Distorts Relative Performance of Constructs. Fluorescence value at 10uM and 100uM divided by basal expression rate in absence of HSL to give Fold Change, error bars denote SEM (n=3). Many systems still show little to no expression at the already very high ligand concentration of 10uM, but exhibit a large jump in expression at 100uM. Since this concentration value is thought to be physiologically irrelevant, fold change based off that concentration can inaccurately describe promoter performance.

fold change) (Figure 2.5A).

Selection of constructs based on EC50 could help create circuits with specific expression dynamics such as sequentially firing promoters based on cell density (Figure 2.5B). Additionally, systems in which the R-protein is completely orthogonal to a ligand until 100uM - since that concentration would be difficult to reach without exogenously provided signal - could be used as a master control of certain systems, allowing for circuits to be triggered only by external input. In general, the EC50 is useful for predicting relative performances of a particular R-protein across ligands. However, it tells you nothing about the raw expression levels, so it isn't the best metric as a standard of performance. For instance, RRR is the most sensitive of all constructs with an EC50 of 0.5nM (Figure 2.5B) but only has a fold change of 28 (Figure 2.5A), meanwhile RLL is three orders of magnitude less sensitive (Figure 2.5B) yet has a fold change of nearly 65 (Figure 2.5A).

The hill slope provides information about how sensitive the R-protein is to its ligand and whether the binding appears cooperative. It is common to attribute digital, or near-digital, responses to QS circuits, but this is inconsistent with the reality of bio-

logical systems, as most canonical QS systems have hill slopes around one (Table 2.1). Nevertheless, synthetic biologists may still want to choose the most digital construct possible (RRR) when constructing their circuit, or possibly the most linear (RLT). In order to quantify and compare the performance of these various QS circuits, activity area was found to be the most useful characteristic. This is consistent with a recent study, which reported AUC to be a better comparison method than EC50 (Huang and Pang, 2012). Activity area includes all aspects of the response curve; that is, less leakiness, greater fold change, higher sensitivity, and lower EC50s all contribute to increasing the activity area (Figure 2.5C, Table 2.1), making it an especially informative performance standard.

Therefore, activity area was used to compare the performances of all of the different systems. As an example, the activity area of LuxR and Plux with an off-target HSL (LLT) was divided by the canonical response (LLL), and it was seen that 3OC8 activated LuxR at 96% of its max efficiency (Figure 2.7A). Similarly, the activity area of RpaR with pC-HSL and the Plux promoter (LRR) was normalized by the response of the canonical lux system (LLL), and it was observed that, at its best, RpaR activated the Plux promoter at 87% of the promoter's maximum observed output over the concentration range in this study (Figure 2.7A). This allows quick evaluation of general properties of these components. For instance, the Plux and Prpa* promoters are promiscuous, while Plas and Ptra* are very specific to their particular R-protein. Unsurprisingly, since the acyl-HSL's of lux, tra, and las are so similar (Figure 1.6), there is a large amount of signal crosstalk between their R-proteins. Conversely, since p-coumaroyl, an aryl-HSL, has a much different structure (Figure 1.1) than the others, it is recognizable by only RpaR, and RpaR cannot recognize the other signals.

The result of this multiplex assay offers insight into many unexpected pairings of receptor, ligand, and promoter that synthetic biologists can utilize for various circuit functions. Since the lux system is widely used, it is important to note that using RpaR with pC-HSL in conjunction with Plux gives an almost identical fold change and hill slope but with higher sensitivity and lower leakiness, making this hybrid system a

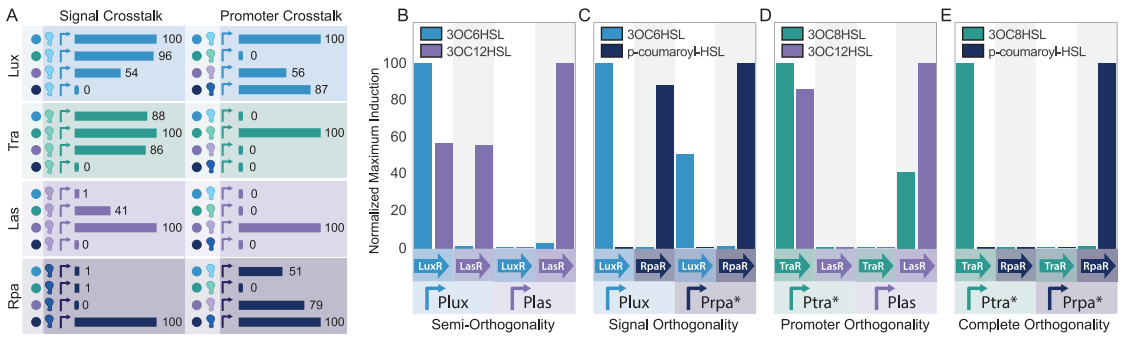

Figure 2.7: Identifying Crosstalk and Orthogonality Between QS Circuits. (*A*) Activity area of the fitted curve, across all HSL concentration values, is used to graphically represent every R-protein's affinity for each HSL ligand and each QS-promoter's ability to be activated by an off-target receptor. Left column: Signal crosstalk as demonstrated by each canonical promoter/R- protein pair's ability to be activated by non-specific ligands. In each box, values are normalized by the maximum performance of that R-protein/Promoter pair (e.g. LLT/LLL = 96%). Right column: Activation of each promoter by each canonical R-protein/ligand pair, representing promoter crosstalk. In each box, values are normalized by the maximum performance of that promoter (e.g. LRR/LLL = 87%). (*B-E*) Comparisons of two sets of QS systems and all possible cross-interactions. Activity area of each column's fitted curve is normalized by the maximum activity area of the promoter corresponding to that particular column (e.g. LLA/LLL or AAL/AAA). (*B*) The lux system demonstrates both signal and promoter crosstalk to the las system, while the las is orthogonal to the lux system. (*C*) The lux and rpa systems are signal orthogonal but demonstrate two-way promoter crosstalk. (*D*) The las and tra systems are promoter orthogonal but demonstrate two-way signal crosstalk. (*E*) The rpa and tra systems are completely orthogonal.

desirable alternative to the canonical lux circuit. Similarly, LasR with 3OC12 driving transcription off the Prpa* promoter is almost half as leaky as the canonical las circuit, while still giving a large fold change and low sensitivity (Table 2.1). Furthermore, comparing the activity area of two QS systems was found to be a useful method to quickly identify crosstalk and orthogonality.

Toward Microbial Consortia

Individual constructs have intrinsic value, however, circuits were evaluated for potential use in multi-system consortia by grouping their cross-interactions (Figure 2.7). Although lux and las have been used in numerous circuits before, they do exhibit a sig-

nificant amount of crosstalk. Specifically, LuxR can become active by binding las's 3OC12, and an activated LasR protein can activate the Plux promoter. However, the Plas promoter is completely orthogonal to the lux system (with the caveat that LasR can become somewhat active at 100uM 3OC6). Taken together the lux/las system exhibits one-way orthogonality (Figure 2.7B) in the physiologically relevant concentration range.

Interestingly, although the lux and the rpa systems exhibited promoter crosstalk, they were signal orthogonal: they could not bind each other's ligand. This crosstalk dynamic implies that they could function independently as long as their promoters are physically compartmentalized (e.g. contained within different cell types, Figure 2.7C). Therefore, a co-culture of lux-responsive and rpa-responsive cells could be orthogonally controlled by their diffusible signal into the 100uM concentration range. The las and rpa systems also exhibited signal orthogonality, with even less crosstalk at 100uM.

There were two system pairs that exhibited signal crosstalk but were promoter orthogonal: the lux/tra pair and the tra/las pair (Figure 2.7D). LuxR and LasR could not activate Ptra*, and TraR could not activate Plux or Plas, however with such similar HSLs, either of the systems' ligand worked to activate both R-proteins to a significant degree. Although signal crosstalk with promoter orthogonality won't explicitly allow for differential control of specific strains, these systems could be used for OR-gates or competitive-inhibition-based circuits (Chickarmane et al., 2007).

Additionally, the tra and rpa systems exhibited both signal and promoter orthogonality, characterizing them as completely orthogonal (Figure 2.7E). These systems would allow for the control of two quorum sensing systems not only in the same culture but within the same cell or compartment. Both R-proteins are incapable of binding to either the non-specific promoter or the non-specific ligand. While signal-orthogonality is sufficient for creating complex population dynamics, assuming each cell is controlled by one system, complete orthogonality can accomplish population dynamics as well as more advanced internal signaling such as the maintenance of two asynchronous, non-interfering oscillators.

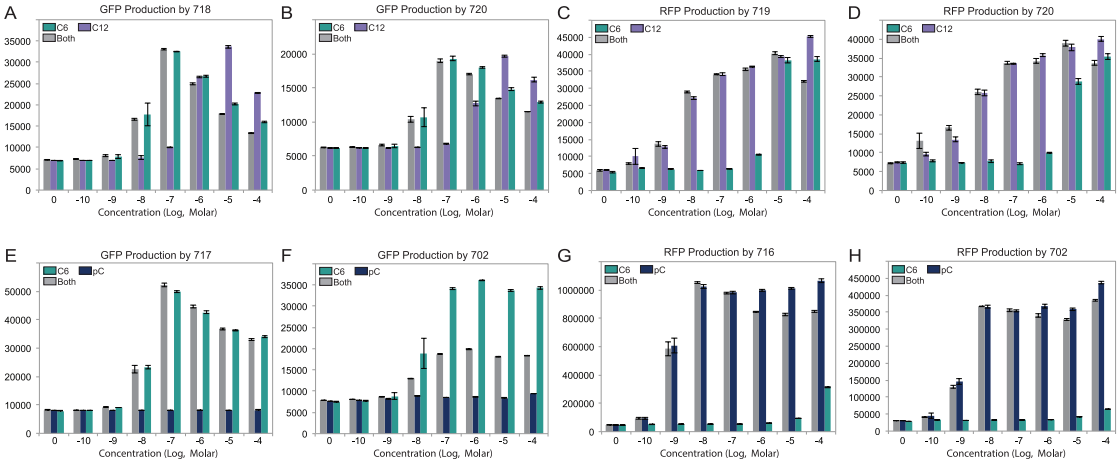

Figure 2.8: Side-by-side Comparison of Raw Fluorescence Expression Between 2-plasmid and 3-plasmid Orthogonality Strains. (A-D) Raw expression from promoter orthogonal strains 718, 717, and 720. (E-H) Raw expression fro complete orthogonal strains 717, 716, and 702. Expression from Strain 717 with C6 and Both is almost identical, however from Strain 702, Both HSLs result in significantly less GFP which is likely a result of growth defects caused by metabolic load of producing RFP at the same time. Error bars represent S.E.M (n=4).

In order to validate the characterization of our constructs and verify their potential for synthetic ecologies, we tested these three communication modules in the same culture or cell (Figure 2.10 and Figure 2.8). Signal orthogonal strains (Figure 2.10A) were co-cultured and exposed to 3OC6HSL (C6), pC, or both HSLs. Their dose-response profiles (Figure 2.10C-D) were used to generate AUC ratios which were compared to response predictions based on the individual constructs previous characterization (Figure 2.10B). The same was done for promoter orthogonal strains (Figure 2.10E-H), and complete orthogonal strains (Figure 2.10I-L) with their respective HSLs.

In all cases, the components behaved very similarly to their predicted response, suggesting these components will translate well into applied circuits. It's important to note that the apparent cross-talk in the GFP-702 column (Figure 2.10J) is due to growth defects. The basal level of GFP remains the same (Figure 2.10K), however the OD decreases with increased pC-HSL (Figure 2.9C) due to the heavy metabolic load of producing RFP and harboring three relatively high-copy plasmids. Since all fluorescence

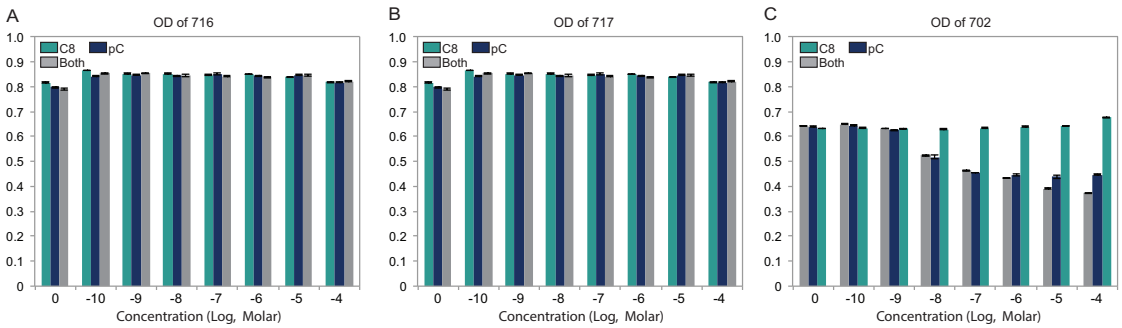

Figure 2.9: Growth Defects Skew Fluorescence Data. Growth defects in the 3-plasmid "Complete Orthogonality" strain 702 compared to the 2-plasmid complete orthogonality strains of 716 and 717. (A-B) OD of strain 716 and 717 3 hours after induction with HSLs. No apparent change in OD due to HSL concentration. (C) Base level OD of Strain 702 is less, likely due to harboring three relative high-copy plasmids. Furthermore, OD decreases with increased concentrations of pC-HSL, likely due to growth defects caused by the production of RFP. These growth defects can distort the meaning of OD-normalized dose-responses. Error bars represent S.E.M (n=4).

data is OD normalized, the subsequent AUC calculations misrepresent a decrease in OD as an increase in OD-normalized fluorescence. These growth defects are likely also responsible for the decrease in GFP production under both HSLs (Figure 2.10K). The complete orthogonality of the rpa/tra systems is further confirmed by Strain 717 which would show the same GFP-AUC ratios as 702 if the cross-talk were real, but having normal growth under all conditions (Figure 2.9B), it more accurately demonstrates tra's unresponsiveness to pC-HSL and RpaR (Figure 2.10J and Figure 2.8E).

Lastly, to further the case for rpa's utility to synthetic biology, we recognize the importance of being able to produce pC-HSL *in vivo*. Preliminary data appears to show that the native sequence from *R. palustris* can be expressed in *E. coli* and activate the Rpa system (Figure 2.11). Further tests are needed to thoroughly prove its functionality, but our data suggests RpaI and the rpa components have potential to be used in future dynamical QS systems.

Characterizing the interactions of just four different quorum sensing systems resulted in the identification of many potential circuit components for use in a variety of synthetic biology applications. Our study demonstrates that because of the natural

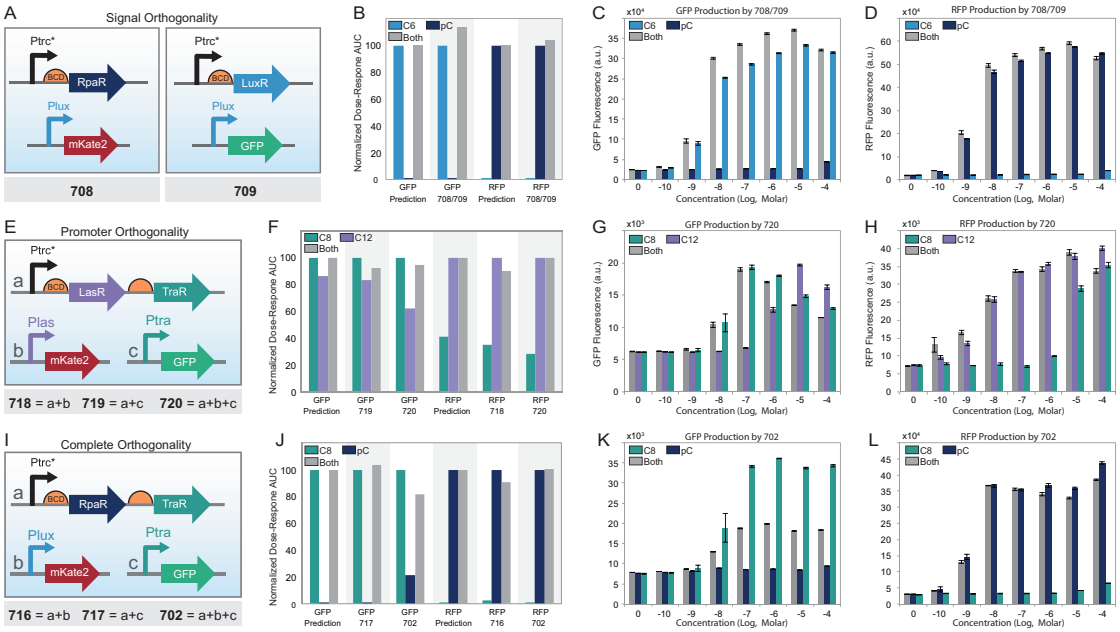

Figure 2.10: Verification of QS Component Orthogonality (*A*) Genetic schematic of signal orthogonal strains 708 and 709. (*B*) A 1:1 co-culture of 708 and 709 was subjected to the full range of HSLs and the AUC of the dose-response was compared to predictions based on their original characterization in Figure 2.4 and Table 2.1. For all predictions, it was assumed the canonical HSL would give the maximum response, so it was assumed providing both HSLs would still give an AUC of 100. Each experiment is normalized by the canonical response, such that the AUC of the GFP dose-response to C6-HSL is set to 100, making the ratio between columns in a set the point of comparison. For example, the 708/709 GFP column set follows this formula: (AUC-C6/AUC- C6), (AUC-pC/AUC-C6), (AUC-Both/AUC-C6). (*C-D*) Raw fluorescence expression of the 708/709 co-culture. Error bars represent S.E.M (n=4). (*E*) Genetic schematic of promoter orthogonal strains 718, 719, and 720. (*F*) Normalized Dose-Response AUC showing similarity between predictions and *in vivo* results. (*G-H*) Raw fluorescence expression of 720. Raw expression of 718 and 719 available in Figure 2.8. (*I*) Genetic schematic of complete orthogonal strains 716, 717, and 702. (*J*) Normalized Dose-Response AUC of predictions and *in vivo* results. (*K-L*) Raw fluorescebce expression of 702. Raw expression of 716 and 717 available in Figure 2.8. Error bars represent S.E.M (n=4).

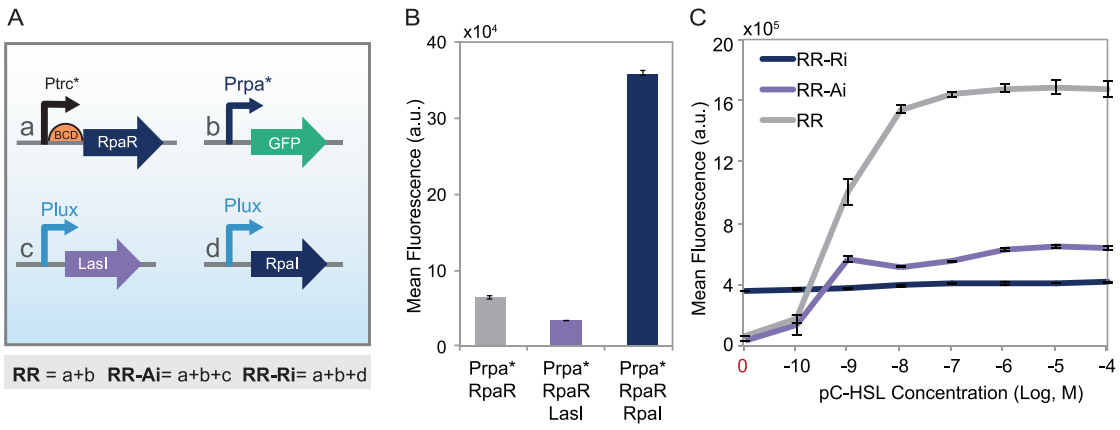

Figure 2.11: Functional Characterization of LuxI-homolog RpaI (A) Genetic schematic of plasmids used, with a a combination of the plasmids a, b, c and d. (B) Inclusion of an RpaI expressing plasmid causes increased GFP expression in an RpaR-expressing strain with GFP driven by the Prpa* promoter. Error bars represent S.D. (n=4). (C) Exogenously providing HSL to the strain with RpaI shows little induction at even the highest concentration of 100uM, hinting that RpaI alone saturates the production capabilities. Raw expression is likely less in the 3-plasmid systems for the same metabolic reasons previously described. Error bars represent S.D. (n=4).

abundance of quorum sensing systems and their ease of engineering, due to protein and promoter modularity, QS is a very attractive tool for the development of next generation genetic circuits and the programming of microbial consortia.

Although completely orthogonal systems have straightforward use cases, we hypothesize that promoter-orthogonal and signal-orthogonal pairs offer their own unique advantages as certain levels of crosstalk may be desirable in creating more interesting circuits with complex dynamics. We anticipate that the unique crosstalk interactions and affinities of the different QS-combinations characterized in this study can be used to this advantage. Furthermore, the possibilities unlocked by QS-circuitry will only grow as more QS systems are characterized and created. Given the ease of promoter and protein engineering of QS components, it is clear that these systems could be further optimized by modifying either the ligand binding, DNA-binding, or sigma-factor-recruiting domains. As more novel QS systems are engineered, the various types and strengths of cross-interaction will be a very useful tool set for real-world applications in synthetic

biology.

Methods

Plasmids and Strains

The plasmids used in this study are described in Table C.2. All studies were done in the "EK" *E. coli* DIAL strain provided by Josh Kittelson (Kittleson et al., 2011); this strain is necessary for proper propagation of plasmids due to R6K and ColE2 origins of replication used in all plasmids. Promoters and UTRs described by Mutalik et al (Mutalik et al., 2013a,b) were synthesized de novo from IDT. Genomes of *Rhodopseudomonas palustris* (RpaR), *Rhodobacter sphaeroides* (CerR), *Sinorhizobium meliloti* (SinR, ExpR), *Serratia marcescens* (SmaR) were obtained from ATCC. Lux, Las and Rhl were obtained in lab and Tra was taken from iGEM pSB1C3-BBa-K916000 found in Distribution Plate 2, Well 9J.

Fluorescence Expression Measurements

Cells were prepared for plate reader experiments as follows: strains were grown overnight and then re-seeded in a 1:1000 dilution into fresh media containing ampicillin and spectinomycin resistance. The dilution was allowed to grow for about 4 hours until it reached OD ~0.1. Then, the cell culture were distributed into a 96-well plate (180ul final volume per well) and induced with a range of AHL concentrations (1:10 serial dilutions were done from 1E-4M to 1E-10M or 1E-14M). AHLs stocks were dissolved in DMSO, resulting in a max DMSO concentration of 1% in LB. After induction, the cells were allowed to grow for 3 hours until OD ~0.5 at which point they were measured with a Tecan infinite M200Pro for OD600 as well as GFP fluorescence with the following fixed settings: no top, fixed gain of 61, excitation of 485nm, emission of 520nm, and Z-position of 19500. All GFP measurements were normalized by dividing their raw values by the OD of that well to give a "per-cell" measurement and account for slight differences in growth rates. For Figure 2.6, the same methods were used, except gain regulation was used to find an optimal gain for each individual experiment, and RFP

Table 2.1: Characteristics of QS Circuit Dose-Responses. Each promoter-R-protein pair has the same leakiness regardless of HSL, so it is only listed once. EC50 was not estimated for constructs with fold changes lower than 2, and any construct that exhibited a greater than 2-fold change only at 100uM was assumed to have an EC50 greater than or equal to 50uM. Hill slopes were only calculated for constructs that showed significant activation before 100uM.

Construct	Dose-Response Curve Properties				
	Leakiness	Fold Change	EC50	Hill Slope	Area
LLL	3.2 ± 0.01	31.5 ± 0.36	4.54E-09	1.15	150800
LLT		32.5 ± 0.12	1.1E-8	0.78	144340
LLA		29.3 ± 0.03	4.75E-7	0.62	81113
LLR		1.3 ± 0.01	–	–	180
LAL	2.08 ± 0.02	3.6 ± 0.45	≥5E-5	–	644
LAT		26.9 ± 0.26	2.08E-06	1.13	35200
LAA		28.6 ± 0.42	1.34E-08	0.69	83782
LAR		2.5 ± 0.28	≥5E-5	–	425
LRL	2.52 ± 0.01	3.1 ± 0.40	≥5E-5	–	402
LRT		2.7 ± 0.07	≥5E-5	–	546
LRA		1.1 ± 0.01	–	–	18
LRR		29.9 ± 0.22	1.37E-09	1.14	131890
TTL	1.74 ± 0.01	5.1 ± 0.06	5.89E-08	1.01	8235
TTT		5.4 ± 0.06	3.16E-08	1.19	9390
TTA		7.1 ± 0.05	9.65E-7	0.86	8067
TTR		1.1 ± 0.01	–	–	43
AAL	3.93 ± 0.01	15.4 ± 2.35	≥5E-5	–	5003
AAT		90.3 ± 0.52	5.95E-7	1.29	279910
AAA		98.7 ± 1.11	1.18E-09	0.94	689740
AAR		8.1 ± 1.55	≥5E-5	–	2639
RLL	2.40 ± 0.01	64.5 ± 0.51	3.15E-7	0.45	156500
RLT		63.0 ± 0.17	2.57E-06	0.41	122680
RLA		19.6 ± 0.16	2.00E-03	0.41	20147
RLR		1.0 ± 0.0	–	–	53
RAL	2.28 ± 0.04	6.6 ± 0.94	≥5E-5	–	1223
RAT		59.8 ± 0.43	1.03E-06	1.12	93241
RAA		62.6 ± 1.45	8.39E-10	0.58	241590
RAR		3.7 ± 0.54	≥5E-5	–	641
RRL	5.71 ± 0.07	7.0 ± 0.73	≥5E-5	–	3551
RRT		6.7 ± 0.11	≥5E-5	–	3839
RRA		1.9 ± 0.20	≥5E-5	–	1036
RRR		27.7 ± 0.12	4.99E-10	1.299	306560

levels were measured with an excitation of 580nm and an emission of 620nm.

Dose-Response Fitting

A Matlab script utilizing nonlinear regression was used to fit the plate reader measurements to the described dose-response equation. The script by Ritchie Smith was obtained here via *mathworks.com* and was slightly modified for this study. The script takes the dose and response matrices as inputs, fits the curve, and outputs the Min, Max, Hill Coefficient, EC50, and AUC of the curve.

Acknowledgements

This material is based upon work supported by the National Science Foundation Graduate Research Fellowship under Grant No. DGE-1144086. Any opinion, findings, and conclusions or recommendations expressed in this material are those of the authors(s) and do not necessarily reflect the views of the National Science Foundation.

Chapter 2 contains material originally published as Scott, Spencer R., and Hasty, Jeff ***ACS Synthetic Biology*** (2016): Quorum Sensing Communication Modules for Microbial Consortia. Copyright permission to republish here was granted by ACS publishing group. The dissertation author was the primary investigator and author on this paper.

Chapter 3

Applications of Multiple Quorum Sensing Systems

Metabolic Distribution

To explore the utility of these systems for industrial applications we took into consideration that attempting to induce strong protein production at an early stage of growth puts a strong selective pressure on a population to foster growth of a mutant with a broken circuit. In order to see if distributing the load across members of a community would alleviate this load-driven mutation problem, we created three strains based on our completely orthogonal QS systems, tra and rpa (Fig. 2.7). One strain (808) only produces RFP in the presence of pC-HSL, the second strain (809) only produces GFP in the presence of 3OC8-HSL, and the third strain (810) produces RFP in the presence of pC-HSL and GFP in the presence of 3OC8-HSL (Figure 3.1A). Each individual strain as well as a co-culture of 808 and 809 was tested under the full concentration of both HSLs to observe growth and expression dynamics. When the

cells are induced right after they are re-seeded (T=0hrs), it causes growth delay that increases with HSL concentration, i.e. induction strength (Figure 3.1B, left column). However, 810 suffers the most as it tries to produce both GFP and RFP while

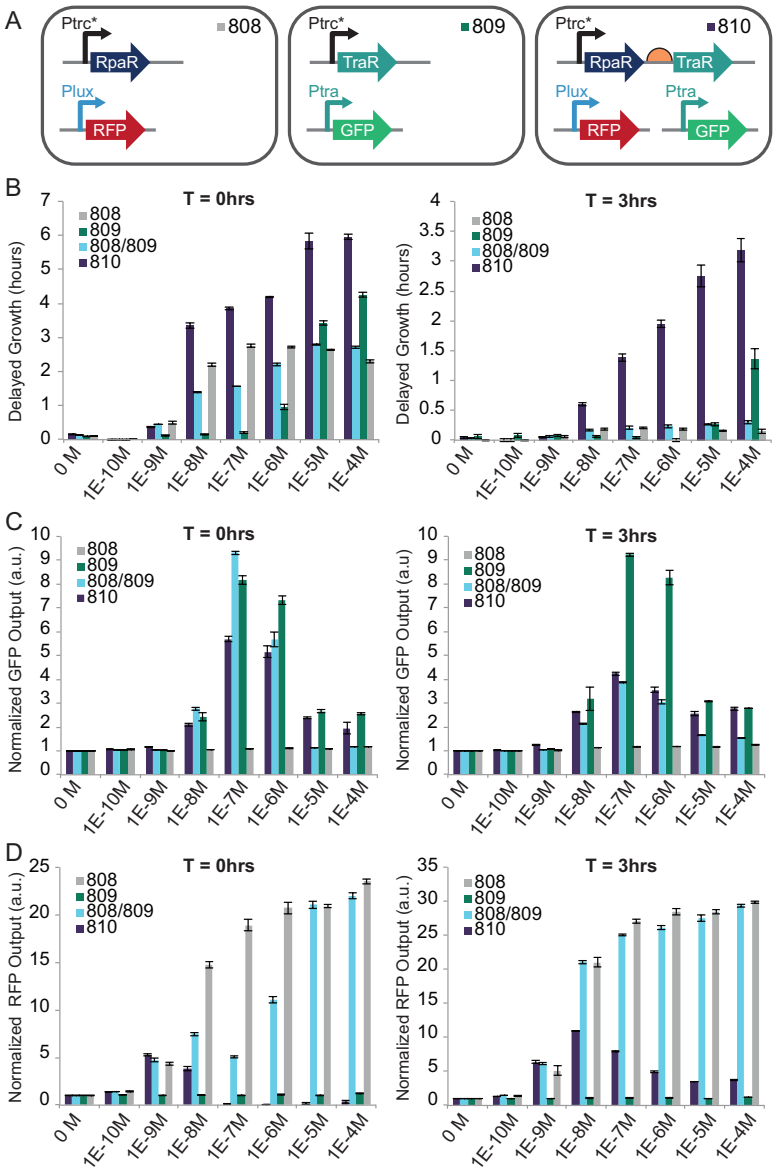

Figure 3.1: Metabolic Load Distribution of QS-Controlled Protein Production. (A) Circuit Diagram for all three strains. In Strain 810, Plux is used in place of Prpa for its preferable dynamics with RpaR - it is also completely orthogonal to the Tra system. (B) For each condition, growth curves were plotted and the resulting time to OD=0.5 was measured. For each strain, the minimum time to OD=0.5 was used as the optimal growth time. Any time greater than that to reach mid-log was considered time of Delayed Growth. Left column: AHL is added right after the cells were re-seeded. Right Column: Cells were grown for 3 hours before being induced. (C) For each strain the GFP signal at each timepoint was summed to give a total GFP production value. That value was then normalized by that strain's uninduced production value (Concentration = 0M). (D) For each strain the RFP signal at each timepoint was added to give a total RFP production value. That value was then normalized by that strain's uninduced production value (Concentration = 0M). For all experiments, n=3 and error bars represent standard deviation from the mean.

the co-culture that demonstrates similar or greater induction values of RFP and GFP grows with much less delay at all concentrations of HSL (Figure 3.1B,C,D, left column). In fact because of this selective pressure, for concentrations higher than 1E-8M, the RFP circuit in the 810 strain is mutated out as demonstrated by the RFP production being lower than the basal non-induced levels (Figure 3.1D, left column). Since one of the advantages of Quorum Sensing is to allow timed production of products at optimal cell-densities (Brockman and Prather, 2015; Srimani and You, 2014; Pai et al., 2012; Tsao et al., 2010), a simulated delayed induction was used to further demonstrate how QS-controlled distributed load would be particularly useful. The growth discrepancies between a co-culture and an overloaded monoculture become even more apparent when the cells are allowed to recover for 3 hours after re-seeding before being induced with HSL. In this case, 810 still exhibits strong growth delays for all concentrations above 1E-9M while none of the other strains are delayed in a comparable way (Figure 3.1B, right column). Interestingly, the co-culture that is grown in the same volume of 810, which therefore has roughly half the number of GFP and RFP producing cells, outperforms 810 in fold induction of RFP in almost all cases (Figure 3.1D, right column), and demonstrates comparable induction of GFP (Figure 3.1C, right column).

Global Toggle Switch

One of the original projects I attempted was to create a toggle switch that synchronizes decision on both the local community level, and "global" population level as was similarly done with synchronous oscillations (Prindle et al., 2012). However, any significant amount of promoter or signal cross-talk would cause both states to be favored at a given time. Therefore, it became clear that complete orthogonality was a prerequisite for creating such a global, quorum-sensing based toggle switch. After identifying the rpa and tra systems as completely orthogonality, the hypothetical toggle switch became much more of an actual possibility. The suggested genotype is described in Figure 3.2, whereby a Plux promoter is controlled by the rpa system and the hybrid

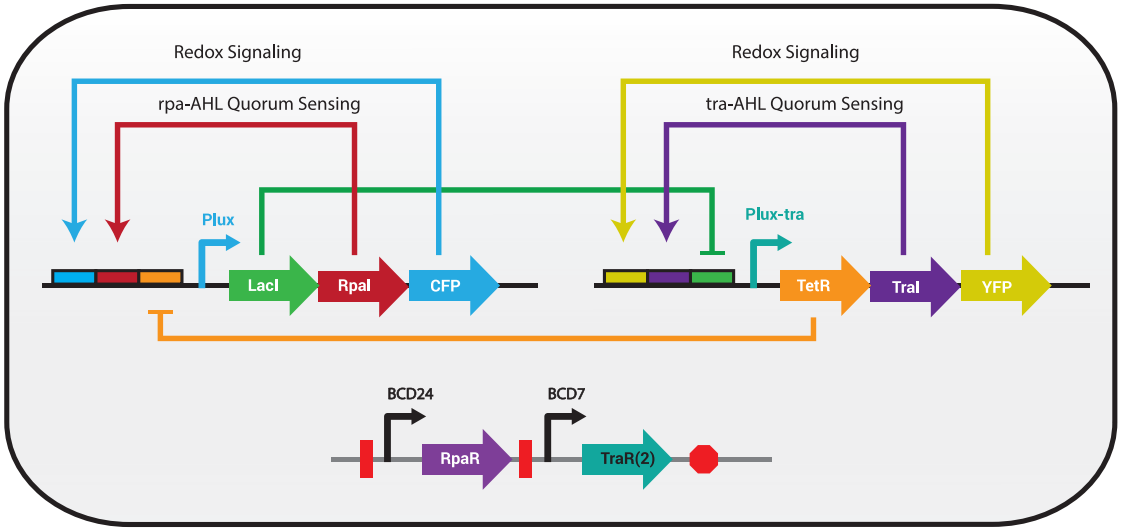

Figure 3.2: Global Toggle Switch Necessitates a Complete Orthogonal Quorum Sensing Pair. Circuit diagram of a globally synched toggle switch. Local, QS-mediated positive feedback achieved with the completely orthogonal rpa and tra systems. Each state is controlled by a hybrid promoter capable of activation by a QS-receptor and a redox-responsive protein. Negative feedback is provided by well-described Lac and Tet repressors.

Plux-tra promoter is controlled by the tra system. Each system also is controlled by a repressor such that while one state favors itself in a positive feedback loop it simultaneously represses the other state.

In situ Multiple, Timed Drug Delivery

In one of the earlier, speculative papers on the advent of microbial consortia, Brenner, You, and Arnold imagined a "healthcare technology requiring the delivery of two therapeutic components in succession with a defined time-offset" that they imagined could use a engineered consortia governed by oscillatory dynamics (Brenner et al., 2008). The first half of this vision was accomplished by Din and colleagues (Din et al., 2016) in their successful use of attenuated *Salmonella* to colonize tumors and administer anti-cancer agents from within in an oscillatory fashion. This bacterial therapeutic utilized the lux quorum sensing system to time periodic lysing events that released an

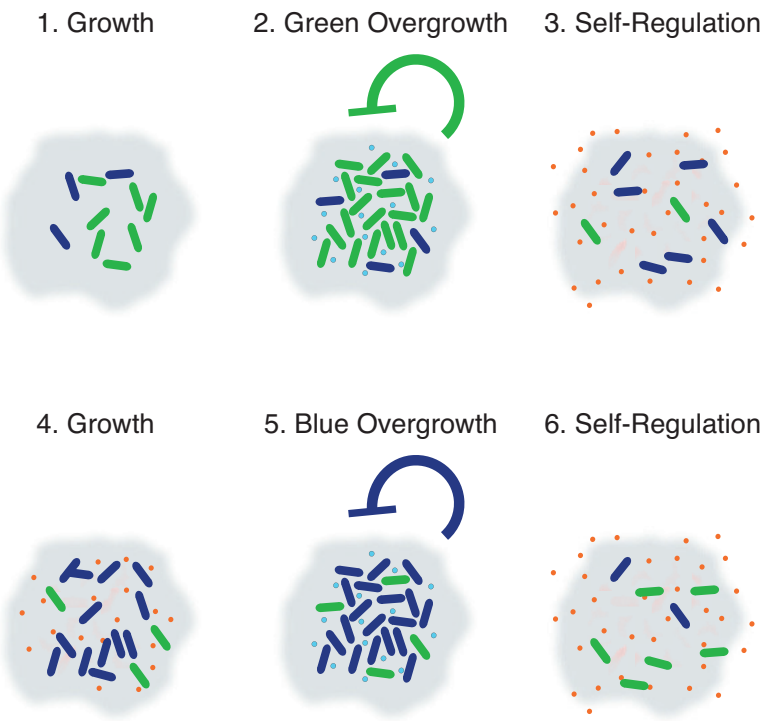

Figure 3.3: Hypothetical Dynamic of a Bacterial Dual Drug Delivery System. Two strains would alternate delivering therapeutic through self-mediated lysis. The first strain would grow to quorum, fire and self-limit. Then the second strain would have space and time to grow until it reached quorum. It would then fire and self-limit. Then the cycle would repeat releasing two therapeutics in succession with an encoded time-offset.

anti-tumor payload. We imagined that if this system were doubled, we could create a two-strain dynamic that delivered two therapeutics with a "defined time-offset", or at least in a successive, periodic manner (Figure 3.3).

The underlying chassis for this hypothetical system were created using two self-lysing strains controlled by the signal orthogonal lux and rpa QS systems an dis described in Chapter 4. While the use of this system could be applied specifically for *in situ* drug delivery, we focus, instead, on its dynamic as a general phenomenon to co-culture two strains that are inherently competitive.

Chapter 4

Engineering Coexistence for competitive strains in a microbial consortia

Introduction

Utilizing reductionism to understand intricate biological systems, ecologists build synthetic microbial ecosystems to study microbial communities (Gravel et al., 2011; De Roy et al., 2013; Tanouchi et al., 2012; Wintermute and Silver, 2010; Klitgord and Segre, 2010), while synthetic biologists use individual genetic "parts" to wire gene networks (Endy, 2005). These interests merge as synthetic biologists and ecologists apply engineered microbial consortia to problems of waste recycling (Fulget et al., 1999), industrial fermentation (Chen, 2011; Patle and Lal, 2007), bioremediation (Dejonghe et al., 2003), and human health (Petrof et al., 2013; Khoruts et al., 2010; Shahinas et al., 2012). However, the progress of engineering microbial consortia has been hindered by the limited ability to co-culture multiple species for long periods of time due to stability issues (De Roy et al., 2014). Here we use a recently developed population control circuit (Din et al., 2016) with novel quorum sensing signaling systems (Scott and Hasty,

2016) to stably co-culture metabolically competitive strains in a microfluidic bioreactor. Previous studies have relied on the ecological regimes of predation (Balagaddé et al., 2008; Kerr et al., 2002) and mutualism (Shou et al., 2007; Kerner et al., 2012; Hillesland and Stahl, 2010; Summers et al., 2010) to stabilize populations; yet recent evidence suggests competition is the most prevalent ecological relation in natural communities (Foster and Bell, 2012; Freilich et al., 2011). Although competitive co-cultures are inherently unstable (Gause, 2003; Faust and Raes, 2012), we found that by using two signal orthogonal quorum sensing systems to direct each strain's self-lysis we drastically improve the residence time of two engineered *Salmonella* strains, compared to the same strains lacking the lysis gene. Agent-based and deterministic modeling of self-limiting bacteria in a microbial consortia demonstrate unique dynamics depending on selected circuit parameters but generally a robust ability to co-culture two competitive species. This system is immediately applicable for further expansion on the periodic *in situ* drug delivery system (Din et al., 2016), but we believe it will be useful for many other aspects of synthetic microbial consortia, from industrial fermentation to understanding natural ecological dynamics.

Results

Exploring the Communication Space of Microbial Consortia

When engineering microbial communities controlled by quorum sensing (QS), the selected receptors and signals will define the communication architecture and determine how the members interact. Generally, a single strain (Green) can either exhibit no communication, inter-communication, intra-communication, or both inter- and intra-communication (Figure 4.1A). The other strain, capable of the same, gives a total of 16 possible communication motifs in a two strain consortia (Figure 1.5). Interestingly, there are certain motifs that require degrees of signal orthogonality such as when each

population only senses its own signal (Figure 4.1A, panel 3). Other motifs can harness cross-talk to their advantage, but still necessitate at least one-way signal orthogonality (Figure 4.1A, panel 4), such as is the case with the canonical lux and las QS systems.

In consideration of these constraints, a representation of previously described quorum sensing systems (Scott and Hasty, 2016) was devised to quickly identify suitable quorum sensing genes for the communication motif of interest. Provided the dose-response curves of a set of quorum sensing receptors to an array of signals (Figure 4.1B), a heat map of the Area Under the Curve (AUC) of their dose-responses can be used to quantify their general behavior (Figure 4.1C). Lumping a receptor-promoter pair as a single receiver and plotting it on one axis, with the signal (HSL) on the other axis creates a heat map with easily extractable information. For instance, taking a 2x2 block from the heat-map will provide a qualitative definition of the signaling properties of a potential two-strain consortia. If all blocks are significantly green then the two systems have two-way crosstalk (Figure 4.1D, left); if all blocks are significantly green except one off-diagonal block, then the systems only have one-way crosstalk (Figure 4.1D, middle). Lastly, if the heat map is a diagonal matrix, then the two systems are signal orthogonal (Figure 4.1D, right). Using this methodology allows quick mapping of real genetic parts to potential communication motifs necessitated by desired community dynamics.

Expanding Self-Lysis Circuit

In an effort to co-culture two strains with possible applications in dual drug delivery, we sought to expand on a recently described synchronized lysis oscillator (Din et al., 2016) and explore its properties in a microbial consortia. The synchronized lysis circuit (SLC) consists of three main modules: the activator module, the lysis module, and the reporter module (Figure 4.1A). All modules are regulated by the luxI promoter which is

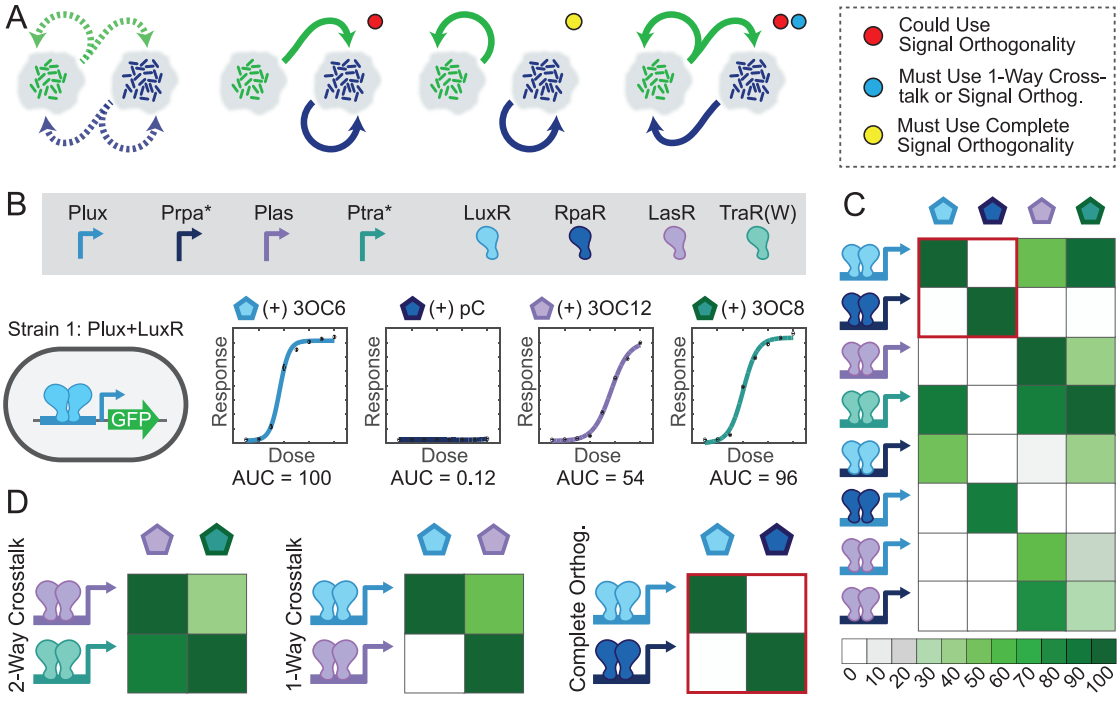

Figure 4.1: Communication Motifs and Quorum Sensing Signaling for Synthetic Microbial Consortia. *(A)* Schematic showing some of the QS communication possibilities between two members of a microbial consortia. (Far left) With each strain capable of either sending, receiving, both or neither, there are generally 16 possible communication motifs. Many of the possible combinations (See Figure 1.5) either necessitate signal orthogonality (middle right) or could take advantage of such systems (middle left and far right). *(B)* Schematic showing how QS systems can be tested and characterized for easy categorization. A strain containing one QS promoter and one QS receptor is subjected toS a range of signals and its dose response curve is quantified by the area under its curve (AUC), which becomes the heat map parameter in C. Signaling homoserine lactones represented as pentagons color-coded to their native QS system. *(C)* Example heat map of aggregated QS systems and their AUC responses to different signals. *(D)* This methodology allows for quick identification of signal orthogonal strains classified by their diagonal matrices. Square matrices with significant induction in all squares indicates two-way signal cross-talk, while one-way signal cross-talk will only have one square not on the diagonal with a significant value.

transcriptionally activated by AHL-bound LuxR. Production of C6-HSL by LuxI thus drives production of the LuxI activator (positive-feedback), the sfGFP reporter, and the bacteriophage lysis gene, ΦX174 E (negative feedback).

Depending on certain parameters of the circuit and chassis, such as growth rate or activator degradation, the lysis circuit can exhibit a variety of lysing dynamics (Figure 4.2B). Scanning through the parameter of activator degradation, the circuit with high degradation (low α_q) exists in the oscillatory phase where the steady-state max and min populations differ from the mean population. As the degradation decreases (α_q increases), the max and min approach the mean, and the circuit enters the constant lysis regime, where the population density settles into a steady-state value.

Conceptually, in the oscillatory lysis regime, a slow build-up of the AHL signalling molecule eventually reaches a threshold level at which point the positive feedback loop activates, and a lysis event reduces the population dramatically. In microfluidic devices, the fluorescent protein sfGFP reports the activation state of the circuit in attenuated *Salmonella enterica subsp. Enterica serovar Typhimurium* (Figure 4.2C). After lysis, a certain number of survivors re-populate the trap, restart the production of AHL, and the process continues in a cyclical fashion (Supplementary Video 1). This dynamic only happens if the degradation is high enough to reset the survivors into the off-state. However, if the degradation is too low, the survivors remain close enough to the AHL concentration threshold that they can never escape the on-state and instead enter the constant lysis regime marked by constant production of sfGFP and simultaneous growth and lysis (Figure 4.2D, Supplementary Video 2).

These dynamics are tunable and relatively predictable by a deterministic model. A model with high degradation (α_q=0.4) shows periodic lysing events (Figure 4.2E, left panel), and the lysis circuit with an LAA-tagged LuxI shows similar lysing dynamics marked by bursts of sfGFP right before and during lysis (Figure 4.2E, right panel). In both cases, the maximum population fills or come close to filling the entire container. Decreasing the degradation (α_q=1.1), the model predicts dampened oscillations, and a LuxI with a TS-linker and an LAA-tag shows a similar dynamic (Figure 4.2F). The

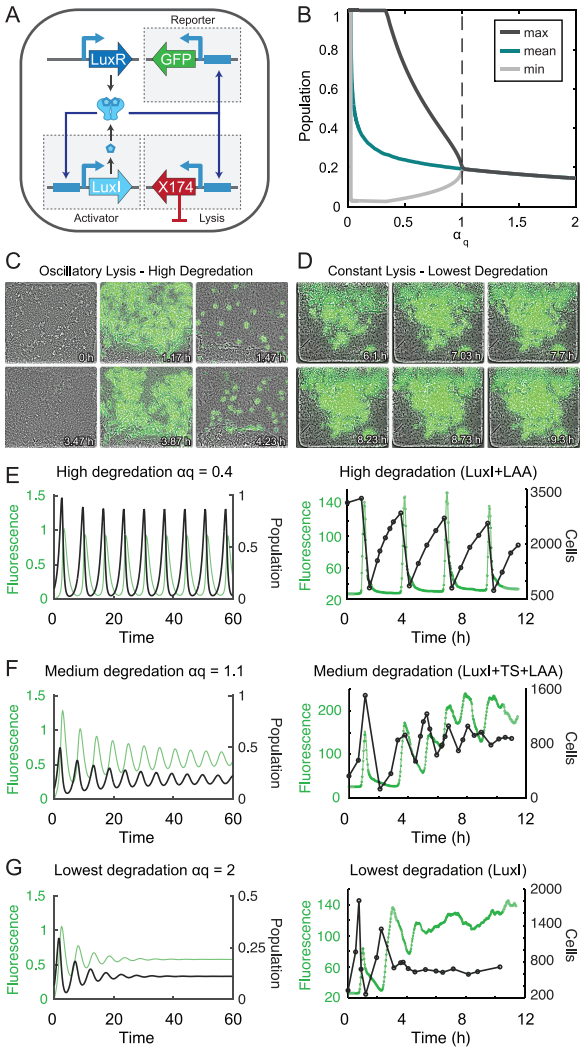

Figure 4.2: Experimental Investigation Into the Space of Population Dynamics of a Self-Communicating Synchronized Lysis Circuit. *(A)* Genetic diagram of the synchronized lysis circuit. *(B)* Parameter scan of LuxI degradation (α_q) plotted against the minimum, maximum, and mean population of bacteria, after a long period of time. *(C)* Video stills depicting the SLC with strong degradation and oscillations. Repeated cycles of growth, quorum threshold reached, and self-limitation by lysis activation. *(D)* Video stills depicting the SLC with weaker degradation and constant lysis. Constant activation of the lysis circuit results in persistent GFP production and a continual balance of growth and death. *(E-G)* Changing certain properties, such as the degradation tag of the SLC will result in different population dynamics. *(E)* Fluorescence (green) and population (black) over time for cells harboring the SLC with α_q=0.4 for the deterministic model and LAA-tagged LuxI for a typical experimental run, as seen in Figure 4.2C. *(F)* Fluorescence (green) and population (black) over time for cells harboring the SLC with α_q=1.1 for the deterministic model and TS-LAA-tagged LuxI for a typical experimental run. *(G)* Fluorescence (green) and population (black) over time for cells harboring the SLC with α_q=2 for the deterministic model and untagged LuxI for a typical experimental run, as seen in Figure 4.2D.

model predicts the maximum population to be significantly less than the full container, and the experimental data's lower cell count matches this prediction. Finally, low degradation (α_q=2) exhibits heavily dampened oscillations and the cells decidedly enter the constant lysis regime. Experimental results from the circuit with an untagged LuxI results in the same dynamics and a maximum population significantly below the size of the container (Figure 4.2G).

These different states are important in establishing how consortia made with this circuit can be altered to change dynamics of a community. More importantly, they showcase that different behaviors can be tuned by easy genetic changes.

Dual-Lysis Population Stabilizing Consortia

To make the consortia of two self-lysing strains, we chose the Lux and Rpa QS systems due to their signal orthogonality demonstrated in Figure 4.1. We used the same lux strain in Figure 4.2 with a CFP reporter and a LAA-tagged LuxI (Figure 4.3A). We then created a similar strain with RpaR in place of LuxR, a LAA-tagged RpaI in place of LuxI, and a sfGFP reporter (Figure 4.3A). These strains are called "Lux-CFP" and "Rpa-GFP", respectively, for convenience. Both strains' gene expression is controlled by the pluxI promoter for consistency, considering pC-bound RpaR can activate pLuxI at about 90% the efficiency of C6-bound LuxR (Figure 4.1C) (Scott and Hasty, 2016).

Although these strains are in the same *Salmonella* chassis, when started from equal densities, Rpa-GFP shows a significant growth advantage over Lux-CFP (Figure 4.3B). Because of this growth advantage, a 1:1 mixture of these strains in a batch culture (with or without the lysis gene), is primarily taken over by the faster growing Rpa-GFP strain by the time the strains reached stationary phase (Figure 4.3C). However, if the slower growing Lux-CFP strain is enriched 100x the green strain, the population stabilizing effects of the lysis circuit becomes evident. Without the lysis gene, the 1:100 mixture is taken over by the blue strain, however with the lysis gene, the population

ratio over the initial 10 hours keeps to around a 50/50 share.

This dynamic becomes evident in the OD curves of the lysis mixtures, whereby the 1:1 mixture only shows the lysis peak of the Rpa-GFP strain, but the 1:100 curve shows both of the lysis peaks (Figure 4.3B). After evidence of the viability of this population stability method, we grew the strains in a microfluidics bioreactor for long-term studies. While each strain alone does nothing out of the expected (Figure 4.6), the co-cultured strains demonstrate unique dynamics. With a seeding ratio of 1:10 (Rpa-GFP to Lux-CFP) the microfluidic trap harboring the two strains without the lysis gene quickly lost its co-culture and was taken over by the Rpa-GFP strain alone (Figure 4.3D) (Supplementary Video 3). This process was repeated for 60 traps, and the time duration of the co-culture was measured over two days. All traps eventually completely lost their co-culture with an average co-residence time of 6.5 hours (Figure 4.3D, bottom panel).

However, when the two lysis strains were grown together, most of the 60 traps maintained a co-culture for the duration of the two-day experiment (Figure 4.3E) (Supplementary Video 4). The addition of the self-lysis module allows the two metabolically competitive strains to cohabit the same container because any "overgrowth" causes a self-limiting lysis event, which gives the other strain space to grow into until it overextends itself and lyses. Due to inherent differences in the kinetics of the genetic circuits, the Rpa-GFP strain remains in the constant lysis regime and is therefore perpetually producing sfGFP. However, the Lux-CFP strain is in the oscillatory regime and remains dark until it reaches quorum threshold and its lysis events are characterized by a short burst of CFP production (Figure 4.3E).

As such, in the fluorescence traces, GFP more or less correlates with the Rpa-GFP population, however, CFP only correlates with the lysis events and not the actual population of the Lux-CFP strain. However, growth of the Lux-CFP strain, as it pushes out the Rpa-GFP strain can be seen by a decrease in the GFP trace, and usually precedes a CFP lysis burst. Experimentally this method seems to stabilize co-cultures strikingly well, especially considering that for the traps that lose their co-culture unfavorable initial conditions caused by the uneven manner of vacuum loading might have caused the

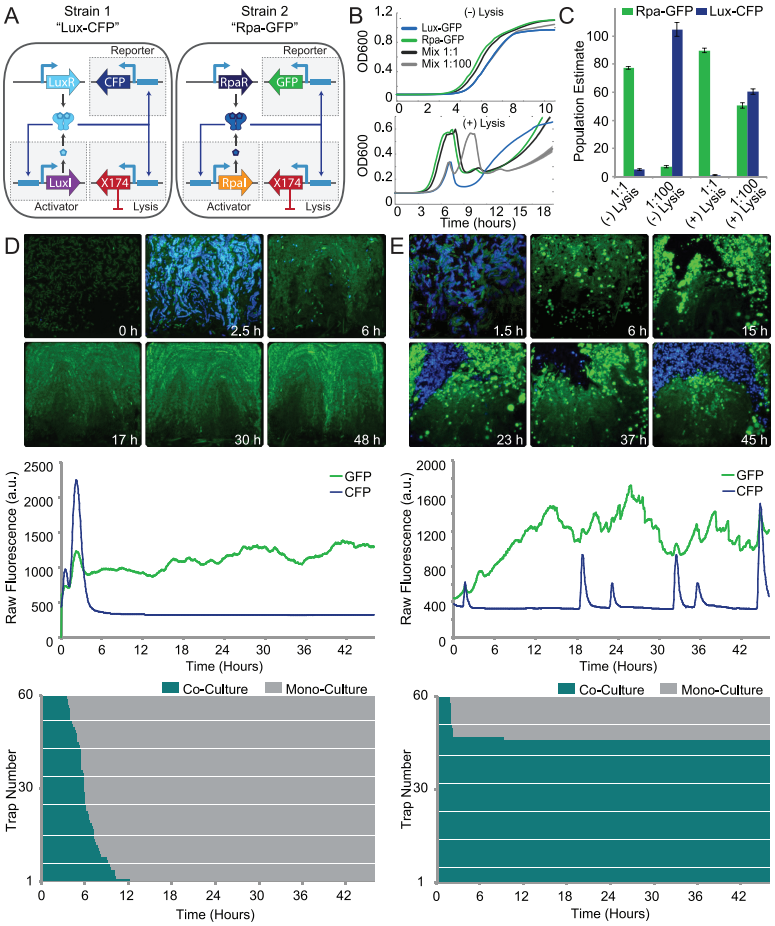

Figure 4.3: Long-Term Co-Culture of Competitive Species with Unequal Growth Rates Using Signal Orthogonal Self-Lysis. *(A)* Genetic diagram of a two-strain consortia of self-lysing *Salmonella* constructed with two signal orthogonal quorum sensing systems, rpa and lux. *(B)* Batch culture growth curves of the Lux-CFP strain alone (blue), Rpa-GFP strain alone (green), a 1:1 mixture (black), and a 1:100 (Rpa-GFP:Lux-CFP) mixture (gray), both without the lysis gene (top) and with the lysis gene (bottom). Width of lines represent s.d. *(C)* Batch culture population estimates of Lux-CFP and Rpa-GFP co-cultures estimated by fluorescence curve normalization, described in detail in the methods section. Error bars represent s.d. *(D)*Video stills of a co-culture of non-lysing Lux-CFP and Rpa-GFP strains showing the eventual takeover by the green strain. Time trace of the GFP and CFP Fluorescence of the trap in the video shown in the middle panel. Sixty traps were monitored over time and their length of co-culture is indicated in the bottom graph. *(E)* Video stills of a co-culture of the Lux-CFP and Rpa-GFP strains with the lysis plasmid. The addition of the lysis plasmid prevents either strain from taking over for the duration of the experiment. Time trace of the GFP and CFP Fluorescence of the trap in the video shown in the middle panel. Sixty traps were monitored over time and their length of co-culture is indicated in the bottom graph.

short residence times. The bimodality of the co-residence time (either lost in the first couple hours, or maintained through the end of the experiment) suggests, given the right initial conditions, this method is rather robust at co-culturing even competitive strains for long periods of time.

Exploring Possibilities with Modeling - Agent-Based

By engineering RpaI with an LAA-tag, we expected oscillations similar to the Lux-CFP strain, however the strain, instead, exhibited constant lysis. We used agent-based modeling to visualize how a co-culture of two orthogonal self-lysis strains in the oscillatory phase would have behaved. In consideration of our experimental parameters, the Rpa-GFP strain grows at 110% the growth rate of the Lux-CFP strain, and the Lux-CFP strain is seeded in a 10:1 ratio to the Rpa-GFP strain. Otherwise, the two strains are identical in the properties of their quorum sensing controlled lysis (Figure 4.4A, Supplementary Video 5). Seemingly due to volume exclusion, as shown by their fluorescence time series, the populations enter an anti-phase pattern where the strains switch off growing and lysing (Figure 4.4C).

Since this dynamic is visually very different than our experimental videos, despite having the expected genotype to create such a dynamic, we modified our agent-based model to demonstrate how the experimental dynamics might have arose. In the second version of the model, several of the Rpa-GFP strain's quorum sensing parameters are changed and the probability of lysing is reduced by 10-fold which allows more HSL to build up and a constant lysis dynamic to develop (Figure 4.4B, Supplementary Video 6). The resulting dynamics were almost identical to the experiment, with a constantly lysing Rpa-GFP strain maintaining the majority of the population share, and the Lux-CFP strain intermittently firing and lysing (Figure 4.4D). In the virtual experiment, GFP "Fluorescence" tracks the population of the Rpa-GFP strain almost exactly since it is constantly green (Figure 4.4D). CFP does not track the population, but only bursts

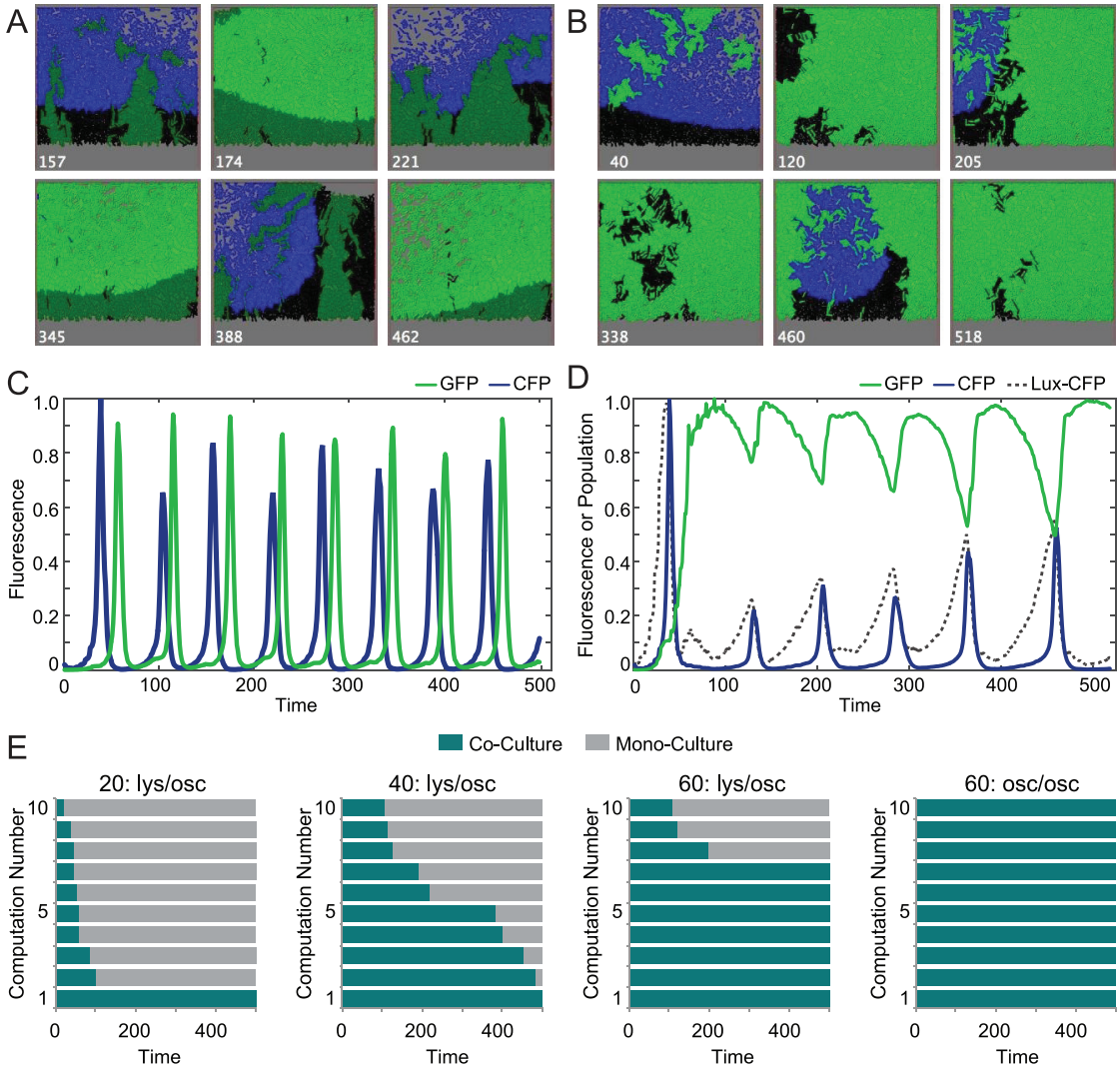

Figure 4.4: Agent-Based Model Elucidating Experimental Dynamics. **A**, Video stills of a virtual co-culture of two self-lysing strains both in the oscillatory regime of the lysis circuit. **B**, Video Stills of model-generated video recreating experimental dynamics. **C**, Time trace of the GFP (green) and CFP (blue) "Fluorescence" of the trap in B over time. **D**, Time trace of the GFP (green) and CFP (blue) "Fluorescence" of the trap in **A**, as well as population of the "Lux-CFP" strain (black, dashed line). **E**, From left to right: (1) green in constant lysis phase, blue in the oscillatory phase in a trap with size 20. (2) green in constant lysis phase, blue in the oscillatory phase in a trap with size 40. (3) green in constant lysis phase, blue in the oscillatory phase in a trap with size 60. Video in B is in this size trap with these lysing conditions. (4) Both strains in oscillatory phase with trap size 60. Video in **A** is in this size trap with these lysing conditions.

when the population reaches high density. Therefore, a decrease in GFP fluorescence, as in the experimental videos, suggests an increase in the Lux-CFP population and will preface a CFP lysis event.

In order to understand how these dynamics, as well as the size of the growth container affects stability the agent-based model was run many times under different conditions. For the experimental-related conditions where Lux-CFP is oscillating and Rpa-GFP is in constant lysis (lys/osc), ten virtual experiments were done in volumes of 20, 40 and 60 each. As the size of the space increases, so does the average residence time of the co-culture (Figure 4.4E), suggesting larger bioreactors will have fewer issues with losing co-culture to stochastic events. Lastly, the dual-oscillating circuit (osc/osc) seems to be extremely robust in its ability to co-culture two strains with all modeling runs maintaining a co-culture for the length of the virtual experiment (Figure 4.4E).

Due to the tunability of the quorum sensing systems and lysis circuit we suspect additional modifications to the real Rpa-GFP strain could push it into the oscillating regime and the resulting dynamics would look like Figure 4.4C, increasing the stability of the co-culture. Envisioning self-lysis as a generalizable control circuit for population stability, further parameters were assessed.

Exploring Possibilities with Modeling - Deterministic

As evidenced by the agent-based model, our strains demonstrate only one particular dynamic of a wide-range of possibilities facilitated by quorum sensing controlled self-lysing microbes. As engineered microbial ecosystems are built with different chassis for specialization purposes, the desired dynamics will change. As such, we created a deterministic model to explore a wider space of possible dynamics achieved through differences in growth rates, QS systems, and lysis circuit regimes (Figure 4.5). For each case, communication motifs as well as real candidate QS systems are distinguished to achieve the displayed dynamic. Furthermore the lysis circuit regime, either Non-lysing,

Lysing, or Weak Lysing is assigned for each strain.

With two non-lysing strains, the faster growing strain will always dominate the population after a certain amount of time (Figure 4.5A). However, if even one of the strains has a self-limiting lysis circuit, a long-term co-culture is possible (Figure 4.5B). In order for this to happen, the non-lysing strain must have a lower growth rate than the lysing strain, but the lysing strain must still be in a regime where activation of lysis causes it to periodically have an effective growth rate lower than the non-lysing strain. In this way, the slow growing non-lysing strain makes up the majority of the population but is periodically displaced by the quicker growing lysing strain before it self-limits with a lysing event.

In cases where both strains harbor a SLC, but there is one-way cross-talk, the strain that responds to both signals becomes entrained to the strain that only responds to its own (Figure 4.5C, 4.5D). The strength of the cross-talk determines the strength and delay of the entrainment, with strong cross-talk (Figure 4.5C) exhibiting strong entrainment, and weak cross-talk (Figure 4.5D) showing time-delayed entrainment.

In cases where each SLC operates independently, by using signal orthogonal QS systems, the most robust co-culturing is achieved (Figure 4.5E). For large ranges of growth rates, the time-averaged population ratio remains around 50/50, making it an especially useful strategy for equally co-culturing two different strains. When growth rates are similar and both strains exhibit oscillatory lysis the dynamics naturally fall into an anti-phase pattern due to volume exclusion as seen in Figure 4.5A. These particular parameters lend themselves most readily to a "healthcare technology requiring the delivery of two therapeutic components in succession with a defined time-offset" imagined by Brenner, You, and Arnold (Brenner et al., 2008) and made realistic by Din and colleagues(Din et al., 2016).

Lastly, the experimental system described in Figure 4.3 and Figure 4.4B was deterministically modeled. It uses two orthogonal self-lysing strains, as in Figure 4.5E, however one of the strains exhibits weaker lysing dynamics, in that it has a lower probability of lysing given a quorum threshold. As seen in the experiment, the Rpa-GFP strain

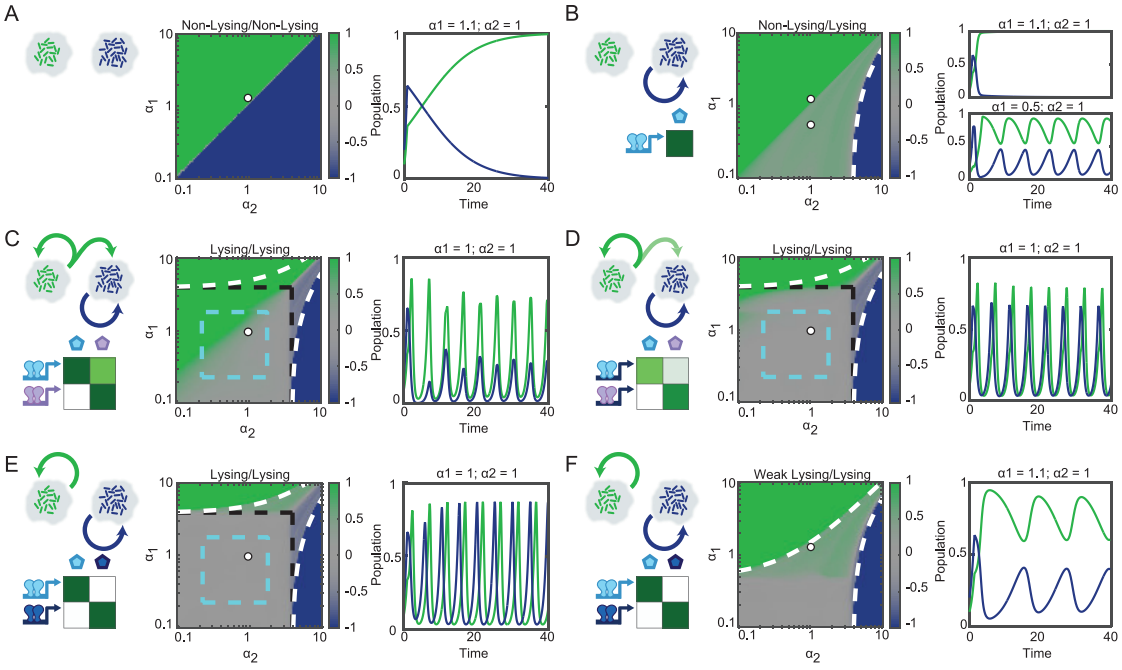

Figure 4.5: Quantitative Prediction of Synchronized Lysis Circuit Dynamics in a Dual Strain Population Using Various Communication Motifs. Model-generated heat map depicting time-averaged population ratio of green and blue strains in a well-mixed, constant flow co-culture, as function of green's growth rate α_1 against blue's growth rate α_2. Each panel has a particular combination of lysis regimes, either non-lysing (Non-Lysing), capable of oscillatory lysing (Lysis), or stuck in constant lysing (Weak Lysis). On the left of each heat-map is the communication motif it exhibits and candidate QS systems to achieve the desired signaling characteristic. These traits determine the behavior and composition of the co-culture. The white dot on the heat map indicates the growth rate parameters selected for the time-series plots. Time series plots show population of the green and blue strains as a function of time. **A**, Two non-lysing strains. **B**, One non-lysing strain and one oscillatory lysing strain. White, dashed lines indicate the growth rate at which one strain's growth rate exceeds that of the other one even for maximum lysis activation. **C**, Two oscillatory lysing strains with one strain having a strong response to the other's QS signal. Cyan dashed lines indicate the region where both strains are in the oscillatory regime, black dashed lines mark the area in which strains are self-limiting. **D**, Two oscillatory lysing strains with one strain having a weak response to the other's QS signal. **E**, Two completely orthogonal oscillatory lysing strains. The rpa and lux systems could be used for this dynamic as they are signal orthogonal. **F**, Two completely orthogonal strains with the Green strain in the constant lysis regime, and the blue strain in the oscillatory lysis regime. This is the regime our experimental system exists.

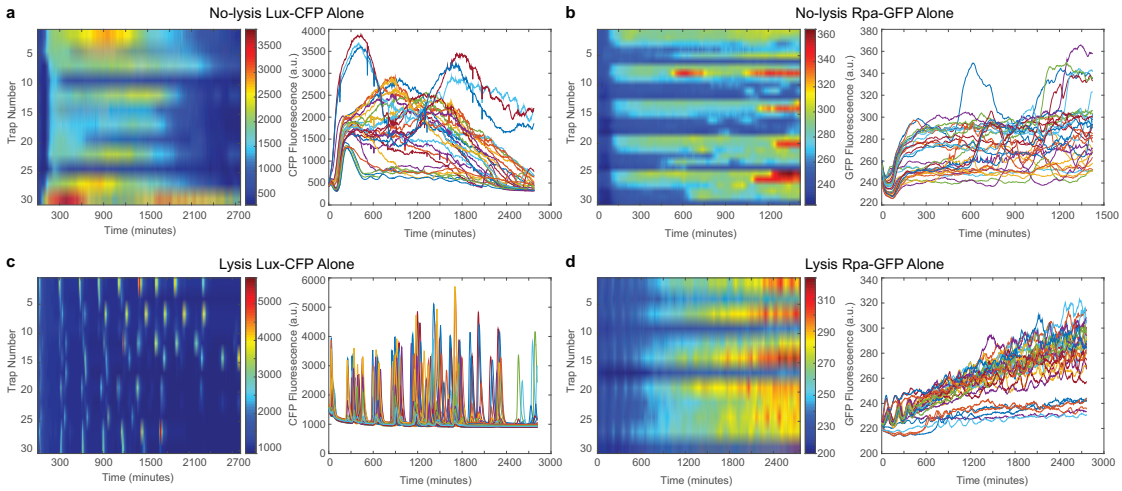

Figure 4.6: Phenotypes of Lysis and Non-Lysis Monocultures. **a** Fluorescence intensity heat map of individual traps plotted against time and raw CFP fluorescence time-series of non-lysis Lux-CFP cells grown alone. **b** Fluorescence intensity heat map of individual traps plotted against time and raw GFP fluorescence time-series of non-lysis Rpa-GFP cells grown alone. **c** Fluorescence intensity heat map of individual traps plotted against time and raw CFP fluorescence time-series of oscillatory lysing Lux-CFP cells grown alone. **d** Fluorescence intensity heat map of individual traps plotted against time and raw GFP fluorescence time-series of constantly lysing Rpa-GFP cells grown alone.

inhabits most of the space, with blue periodically displacing it until it reaches quorum and self-limits its population. This dynamic, as each dynamic does, offers a distinct advantage for certain purposes. A system requiring a constant production of a particular chemical and periodic bursts of a second chemical could appropriate this system to its advantage.

Discussion

Synthetic biologists have used lysis to control populations before (You et al., 2004), but not until recently (Din et al., 2016) have populations been engineered to control their own population without exogenous input. Moreover, recent evidence has identified quorum-sensing controlled self-lysis as a naturally occurring phenomenon in *Pseudomonas aeruginosa* (Zemke and Bomberger, 2016), which is a perfect example of how the interests of synthetic biologists and microbial ecologists are merging in the field of engineered microbial ecosystems. This duality suggests that not only will this dynamic be useful for synthetic biology applications, it may help studies into the dynamics of natural ecosystems.

With the additional modeling of our circuit it becomes clear that the transition from monoculture synthetic biology to synthetic engineered ecosystems will be marked by an explosion of possibilities. A circuit designed for monocultures, such as the SLC, can have drastically broadened use-cases when expanded into the setting of a community. This phenomenon of stably co-culturing two metabolically competitive strains through orthogonal self-lysing offers many unique applications in itself but also represents the complexity communities are capable of achieving beyond their monoculture predecessors.

Supplementary Movies

Supplementary Videos are available through ProQuest and will be available through Nature or other publisher in the eventuality of the work in Chapter 4 being published.

Materials and Methods

Plasmids and Strains

Our circuit strains without the lysis plasmid were cultured in LB media with 50 μg ml^{-1} kanamycin, in a 37 °C incubator. Our circuit strains with the lysis plasmid were cultured in the same way but with 34 μg ml^{-1} of chloramphenicol as well along with 0.2% glucose. For microscopy and plate reader experiments 1nM of 3-oxo-C6-HSL was added to all media. Plasmids were constructed using the CPEC method of cloning or using standard restriction digest/ligation cloning. The lux activator plasmid (Kan, ColE1) and lux-lysis plasmid (Chlor, p15A) were used in previous work from our group (Prindle et al., 2012; Din et al., 2016). The RpaR and RpaI genes were obtained via PCR off the *Rhodopseudomonas palustris* genome obtained through ATCC to create the rpa-activator and rpa-lysis plasmids. The lux-lysis circuit alone was characterized in *E. coli*. Co-culturing was performed with non-motile *S. typhimurium*, SL1344 (Table C.3).

The Lysis circuit, in both the Lux and Rpa case, is composed of an activator plasmid and a lysis plasmid. For the circuit characterization experiments there were three variations of the activator plasmid. The first is pTD103LuxI-sfGFP which was used in previous work from our group (Prindle et al., 2012). This plasmid contains a LuxI with the ssrA-LAA degradation tag (amino-acid sequence of AANDENYALAA) and sfGFP, a superfolding green fluorescent protein variant (Pédelacq et al., 2006). pTD103LuxI (TS) sfGFP was constructed by adding the TS-linker (amino acid sequence of TS) between the ssrA-LAA tag and LuxI. pTD103LuxI (-LAA) sfGFP was constructed by removing the ssrA-LAA tag from LuxI. For the dual lysis experiments, the Lux-CFP strain used the activator plasmid with the ssrA-LAA tagged LuxI but with a CFP in

place of the sfGFP. The Rpa-GFP strain's activator plasmid was created by replacing LuxR with RpaR and the LuxI with an ssrA-LAA tagged RpaI.

The lysis plasmid have a p15a origin of replication and a chloramphenicol resistance marker (Lutz and Bujard, 1997) and have been previously described by our group (Din et al., 2016). The lysis gene, E from the bacteriophage ϕX174, was kindly provided by Lingchong You and was taken from the previously reported ePop plasmid via PCR (Marguet et al., 2010). The E gene was placed under the expression of the LuxR-AHL activatable luxI promoter for both the Lux-CFP and Rpa-GFP strains. Most of the construction was done using the CPEC method of cloning (Quan and Tian, 2009). See Extended Data Fig. 5 for maps of the the plasmids used in this study.

Microfluidics and Microscopy

The microfluidic devices and experiment preparation protocols used in this study are similar to those previously reported from our group (Prindle et al., 2012). The bacteria growth chambers were 100μm wide 85μm deep and approximately 1.6μm in height. For single strain experiments on the chip, mid-log cultures were spun down in a micro centrifuge and loaded via vacuum pressure. For co-culture experiments on the chip, strains were seeded from -80 cultures and grown until an OD $\sim$0.2, spun down, mixed at a 10:1 ratio (Lux-CFP:Rpa:GFP) and loaded via vacuum pressure. Acquisition of images was performed with a Nikon TI2 using a Photometrics CoolSnap cooled CCD camera. The scope and accessories were programmed using the Nikon Elements software. Co-culture was determined to be lost if the fluorescence of either CFP or GFP went below background fluorescence, and then was checked manually in cases of the oscillatory lysing CFP strain which can go below threshold between lysis events. Additional information on microfluidics and microscopy can be found in Appendix A.

Our group has previously described in depth the microscopy and microfluidics techniques used in this study (Danino et al., 2010). In short, micron-scale features are baked onto silicon wafers using cross-linked photoresist. The microfluidic device resin, PDMS (polydimethysiloxane), is then poured over the wafers and solidified by baking. The

PDMS, whcih contains numerous devices, is peeled off and individual devices are cut out from the whole. Holes are then punched into the device at their input and output where the fluid lines will eventually plug in. After puncturing, the devices are bonded onto glass coverslips via plasma-activation. The devices were then put in a vacuum and the outlet was loaded with cells and the inlet with media. Vacuum pressure loads cells into the traps and media lines are plugged in before the cells can contaminate the upstream section of the device. The flow was then adjusted by changing the relative heights of the syringes, which for all experiments the meniscus of the media was set to one inch above the meniscus of the waste, resulting in a low, constant hydrostatic pressure driven flow.

All microfluidic experiments were done in a side-trap array device as previously described(Danino et al., 2010), and in all cases 0.075% Tween20 was added to the media to deter cells from sticking to the channels and the ports of the device.

For lysis characterization (figure 2): Cells were cultured until they reached an optical density of approximately 0.1 (Plastibrand 1.5mL cuvettes were used) at which point they were spun-down and loaded into the chip. Media was LB with Kanamycin and Chloramphenicol.

For dual lysis and co-culturing experiments (figure 3): Cells were cultured until they reached an optical density of approximately 0.1 (Plastibrand 1.5mL cuvettes were used to test OD) and 1.5mL was spun down and resuspended in 50ul of media. This concentrate was used to vacuum load the cells for single strain experiments, or it was mixed together before loading in the co-culturing experiments. Media was LB with Kanamycin (and Chloramphenicol for lysis experiments) with 1nM 3OC6 HSL added.

The microscope system used has also been previously described by our group (Prindle et al., 2012). In short, a Nikon Eclipse TI epifluorescent microscope with phase-contrast based imaging was used. Our camera is a Photometrics CoolSNAP HQ2 CCD.

The acquisition software used is Nikon Elements. Our microfluidic devices are housed in a plexiglass incubation chamber that is maintained at 37C by a heating unit.

For dual lysis and co-culturing experiments: Phase-contrast images were taken at 20x

magnification with 50-200ms exposure times. Fluorescent imaging at 20x was performed at 300ms for GFP, 30% setting on the Lumencor SOLA light source, and 300ms and 35% for CFP. Images were taken every 3 minutes for the course of the experiment ($\sim$2 days). The Data Analysis section below discussed the analysis of these images further.

Plate Reader Fluorescence and Population Estimates

For the well-plate experiments the strains were grown in a standard Falcon tissue culture 96-well flat bottom plate with appropriate antibiotics (kanamycin only for non-lysis and kanamycin and chloramphenicol for lysis strains). For consistency with microfluidic experiments, 1nM of 3OC6-HSL was added to all media. We grew the bacterial strains listed in Fig. 3b in 4mL cultures to an optical density of 0.15 before adding 10uL of this culture to 10mL of fresh LB with appropriate antibiotics and added HSL. For single strain tests, 200ul of the dilution was distributed into the well-plate. For the 1:1 mixtures, 100ul of each dilution was added to the same well. For the 1:100 mixtures 200ul of the Lux-CFP dilution was added with 2ul of the Rpa-GFP dilution. For all cases there were four technical replicates.

These dilutions were then grown for 10 hours (non-lysing), or 19 hours (with lysis) and their OD600nm, GFP, and CFP levels were measured every 10 minutes in a Tecan Infinite M200 Pro. GFP readings had an excitation of 485nm and emission of 520nm. CFP readings had a an excitation of 433nm and emission of 475nm.

Data Analysis: Well-plate Experiments

Population estimates in the co-culture mixtures was estimated in the following way. The GFP fluorescence time-series trace of Rpa-GFP alone was integrated and used as a standard for accumulated fluorescence of a culture with 100% of the Rpa-GFP strain. In the same way, the CFP fluorescence time-series trace of Lux-CFP alone was integrated and used as a standard for accumulated fluorescence of a culture with 100% of the Lux-CFP strain. The integrated GFP and CFP fluorescence curves of the mixtures was

then divided by the standards to give a population estimate of Rpa-GFP and Lux-CFP, respectively. For all cases, the area of the background fluorescence was subtracted. Additionally, the GFP fluorescence required extra signal normalization because the Tecan's GFP sensor reads into the CFP emission profile (but not the other way around).
Here are the equations used to calculate the population estimates with appropriate filtering and normalization:

$$\begin{aligned}
Population_{Lux} &= \frac{Area(CFP_{mix}) - Area(BG_{CFP})}{Area(CFP_{Lux}) - Area(BG_{CFP})} \\
\eta &= \frac{Area(GFP_{Lux}) - Area(BG_{GFP})}{Area(CFP_{Lux}) - Area(BG_{CFP})} \\
GFP_{Crosstalk} &= [Area(GFP_{mix}) - Area(BG_{GFP})] \\
GFP_{Real} &= GFP_{Crosstalk} - [Area(CFP_{mix}) - Area(BG_{CFP})]\eta \\
Population_{Rpa} &= \frac{GFP_{Real}}{Area(GFP_{Rpa}) - Area(BG_{GFP})}
\end{aligned}$$

$Population_{Lux}$ is the population estimate of the Lux-CFP strain in a co-culture.
$Area(CFP_{mix})$ is the area of the CFP fluorescence time-series curve of a given co-culture. $Area(BG_{CFP})$ is the area of the background CFP fluorescence time-series line. $Area(CFP_{Lux})$ is the average area of the CFP fluorescence time-series curve in the wells with only the Lux-CFP strain. $Area(GFP_{Lux})$ is the average area of the GFP fluorescence time-series curve in the wells with only the Lux-CFP strain (For this strain the GFP fluorescence should technically be at background, further normalization is done because the Tecan's GFP sensor reads into the CFP emission profile). $Area(BG_{GFP})$ is the area of the background GFP fluorescence time-series line. η is the calculated fluorescence emission cross-talk scalar, and is only needed to scale GFP values as the CFP sensor does not read any GFP. The normalized, filtered, GFP value is thus given by GFP_{Real}. $Area(GFP_{mix})$ is the area of the GFP fluorescence time-series curve of a given co-culture. $Area(GFP_{Rpa})$ is the average area of the GFP fluorescence time-series

curve in the wells with only the Rpa-GFP strain. Finally, $Population_{Rpa}$ is the population estimate of the Lux-CFP strain in a co-culture.

Data Analysis: Microfluidics

We counted cells using the following strategies: For experiments where the cell population was mostly aggregated together (non-sparse population), we first estimated the average area of an individual bacterial cell and the average void fraction (open space between bacteria in the trap). Taking into account the pixel density of the image, we measured the area of the trap taken up by cells using ImageJ and divided by the average area of a bacterial cell. This value was then multiplied by (1 - void fraction) to yield the total estimated number of cells in the trap. Bacteria that were not close to the main group of cells were counted individually and added to the final number. For experiments where the growing population was sparse (due to the constant lysis regime), we utilized the Trainable Weka Segmentation plug-in for ImageJ to count cells. Plots were generated by using MATLAB.

For co-culture experiments: Co-culture was determined to be lost if the fluorescence of either CFP or GFP went below background fluorescence, and then images were checked manually in cases of the oscillatory lysing CFP strain which can go below threshold between lysis events.

Agent-Based Modeling

Images and data in Fig. 4.4 were generated using an agent-based model which combines the ordinary differential equation model from (Din et al., 2016) that describes the intracellular dynamic behavior of the synchronized lysis circuit with the agent-based model (Volfson et al., 2008)(Mather et al., 2010) describing the division and motion of cells. More information and the governing equations can be found in Appendix A.

Deterministic Modeling

For the parameter scan of a single strain in Figure 4.2, the model equations (see Ap-

pendix A for details) were simulated for 2000 time units for different values of the model parameter α_q. The last 160 time units were used to determine the minimum, mean and maximum population density. For all parameter scans of two strains, the model equations were simulated for 500 time units and the last 100 time units were analyzed to determine the average cell densities $\bar{n}_1$ and $\bar{n}_2$ of the two strains. The "steady-state population ratio" shown in Figure 4.5 was then calculated as $(\bar{n}_1 - \bar{n}_2)/(\bar{n}_1 + \bar{n}_2)$, ranging from -1 (strain 2 dominates) to 1 (strain 1 dominates). For non-lysing strains, the model parameter q_c was set to infinity. Cross-talk parameters in Figure 4.5C and D, are $\xi = 0.6$ and $\xi = 0.12$, respectively. Weak lysis (strain 1, Figure 4.5F) was achieved by reducing the lysis rate of the strain to $\gamma = 0.5$. More information and the governing equations can be found in Appendix B.

Acknowledgements

Chapter 4 contains material being prepared for submission as Competitive Species Stably Co-Cultured in a Synthetic Microbial Ecosystem Through Orthogonal Self-Lysis. Scott, Spencer R., Din, M. Omar, Bittihn, Philip, Xiong, Liyang, and Hasty, Jeff. The dissertation author was the primary investigator and author on this paper.

Chapter 5

Summary and Conclusion

As synthetic biologists, we seek to uncover and reimagine the inherent power of natural systems. Evolution has encoded powerful capabilities into the DNA of diverse organisms, and it's synthetic biology's job to both understand those capabilities and re-purpose them to build sustainable technologies and next-generation therapeutics. In this thesis I describe why further advancements in the field will require the use of a community or synthetic ecosystem of organisms working together to accomplish more complex tasks. These communities will rely on well-defined communication systems, and the quorum sensing systems we developed and described are designed to meet that need. We also were careful to find the most useful way to present the characteristics of QS system sin the context of a microbial consortia, deciding on the AUC heatmap as the quickest way to label pairwise QS systems with their paradigm or communication module. We explained why these modules are important by highlighting that certain communication motifs require a particular orthogonality characteristic. This became important when applying these systems for the real-world application of creating a dual-delivery bacterial therapeutic. Finally, in creating this therapeutic, we described a dual-lysis system that allow for the long-term coexistence of competitive strains. Looking forward into the future of synthetic biology, we imagine that increased coexistence methods and communication systems will allow for the construction of synthetic ecosystems capable

of tackling the worlds most complex problems of sustainability and health.

Appendix A

Agent Based Modeling

For the agent-based model, to simulate bacterial motion, we adapted the mechanical agent-based model developed in our earlier work(Volfson et al., 2008)(Mather et al., 2010). Each cell is modeled as a spherocylinder of unit diameter that grows linearly along its axis and divides equally after reaching a critical length $l_d = 4$. It can also move along the plane due to forces and torques produced by interactions with other cells. The slightly inelastic cell-cell normal contact forces are computed via the standard spring-dashpot model, and the tangential forces are computed as velocity-dependent friction.

To describe the intracellular dynamics of each cell, we adapted the ordinary differential equation model from(Din et al., 2016). Specifically, the intracellular dynamics are

$$\begin{aligned} P_{lux} &= \alpha_0 + \alpha_H \frac{(\frac{H_i}{H_0})^m}{1+(\frac{H_i}{H_0})^m} \\ \frac{dH_i}{dt} &= b\frac{I_i}{K_I + I_i} + D_m(H_e(\mathbf{x}_i,t) - H_i) \\ \frac{dI_i}{dt} &= C_I P_{lux} - \gamma_I I_i \\ \frac{dL_i}{dt} &= C_L P_{lux} - \gamma_L L_i \end{aligned}$$

Here the variables P_{lux}, H_i, I_i and L_i are the activity of luxI promoter, intracellular AHL, LuxI and lysis protein of the i-th cell. $H_e(\mathbf{x}_i,t)$ is the extracellular concentration of AHL at the location of the i-th cell. luxI promoter is induced by AHL. $b\frac{I_i}{K_I+I_i}$ is the production term for AHL. $D_m(H_e(\mathbf{x}_i,t)-H_i)$ describes the exchange of intra- and extra-celluar AHL across the cell membrane. $C_I P_{lux}$ and $\gamma_I I_i$ are the production and degradation terms for LuxI. $C_L P_{lux}$ and $\gamma_L L_i$ are the production and degradation terms for lysis protein.

The extracellular AHL concentration $H_e(\mathbf{x},t)$ is governed by linear diffusion equation

$$\frac{\partial H_e(\mathbf{x},t)}{\partial t} = D_m(\sum H_i\delta(\mathbf{x}-\mathbf{x}_i) - H_e(\mathbf{x},t)) - \delta_H H_e(\mathbf{x},t) + D_H\nabla^2 H_e(\mathbf{x},t)$$

In the simulation, we use 2D finite difference methods to describe the diffusion of AHL.

We implement the model in traps with diffrent side lengths (20, 40 and 60). To simulate the lysis of each cell, we assume that when the concentration of lysis protein L_i is above a threshold L_{th}, the cell has a probability of $P_r = p_L(L_i - L_{th})$ per unit of time to lyse and once a cell lyses, it is removed from the trap.

We chose model parameters to qualitatively fit the experimental results and the parameters H_0, m, b, p_L were chosen to account for the differences of experimental measurements and dynamic behaviors between Lux-CFP and Rpa-GFP strains. The parameter values for the Lux-CFP strain are $\alpha_0 = 0.1$ (Lux promoter basal production); $\alpha_H = 2$ (Lux promoter AHL induced production); $H_0 = 1$ (AHL binding affinity to Lux promoter); $m = 4$ (Hill coefficient of AHL induced production of Lux promoter); $b = 1.5$ (AHL production rate); K_I (Conc. of LuxI resulting half maximum production of AHL); $D_m = 10$ (Diffusion constant of AHL across cell membrane); $C_I = 1$ (LuxI copy number); $\gamma_I = 1$ (Degradation rate of LuxI); $C_L = 1$ (Lysis gene copy number); $\gamma_L = 0.5$ (Degradation rate of lysis protein); $\delta_H = 0.1$ (Dilution rate of extracellular AHL); $D_H = 65$ (Diffusion constant of extracellular AHL); $p_L = 0.3$ (Probability of lysing); Ł$_{th} = 1.6$ (Threshold of lysis protein for lysis).

To simulate the constant-lysis Rpa-GFP strain, these parameters have different values: $H_0 = 0.2, m = 1, b = 0.8, p_L = 0.03$. Besides, Rpa-GFP strain's growth rate is

10% larger than Lux-CFP strain.

Appendix B

Deterministic Modeling

Single lysis oscillator strain

We describe the population level mechanisms that lead to oscillations in population size as observed with the synchronized lysis circuit. To gain an intuitive understanding, we use a reduced model that aims to reproduce the observed population level behavior using only the fundamental ingredients of the circuit: Autocatalytic production of quorum sensing agent and quorum sensing agent-induced lysis of cells. The basic equations for a single strain equipped with the lysis circuit are as follows:

$$\frac{\mathrm{d}n}{\mathrm{d}t} = \alpha n - f(q)\gamma n \tag{B.1a}$$

$$\frac{\mathrm{d}q}{\mathrm{d}t} = [\alpha_q + \alpha_q^* f(q)]n - \gamma_q q \tag{B.1b}$$

The cell density is denoted by n. Cells divide with a rate α and die with a maximal rate γ due to lysis. $0 \leq f(q) \leq 1$ characterizes the promoter under which the QS and lysis proteins are expressed, so it determines the dependence of the death rate on q and the auto-catalyzed production of the QS agent q. α_q is the basal production rate of QS agent, which can be increased by the presence of q to a maximum production rate of $\alpha_q + \alpha_q^*$. q is diluted in the environment with a rate γ_q. We use a standard Hill function

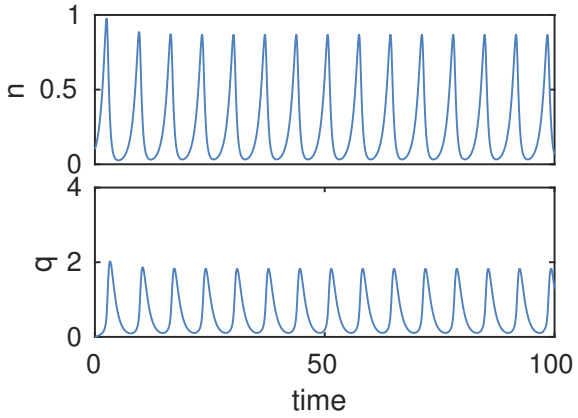

Figure B.1: Dynamics of the model equation $B.1$.

for $f(q)$:

$$f(q) = \frac{q^m}{q_c^m + q^m}, \tag{B.2}$$

where q_c is the concentration of q that induces results in the half-maximum death rate (and auto-catalyzed production of q) and m is the Hill coefficient.

A linear stability analysis shows that the system $(1a)$ has a stable fixed point when

$$m\left(1 - \frac{\alpha}{\gamma}\right) < 1 + \frac{\alpha_q \gamma}{\alpha_q^* \alpha}. \tag{B.3}$$

The border of this stability region corresponds to the onset of oscillations. Basal parameters are, unless otherwise mentioned: $\alpha = 1$, $\gamma = 4$, $\alpha_q = 0.4$, $\alpha_q^* = 8$, $\gamma_q = 1$, $q_c = 1$, $m = 2$. These parameters lead to oscillations according to equation $B.3$. All simulations are carried out using the Runge-Kutta-Fehlberg (RKF45) method. An example trajectory is depicted in Figure B.1.

While we do not explicitly model individual proteins or enzymes, we can gain an understanding for the influence of LuxI degradation by ClpXP with the model equation $B.1$ using the following logic: When there is very little LuxI (i.e. the positive feedback loop has not been activated), fast degradation by ClpXP will have a strong influence on the steady-state level of LuxI. LuxI with a strong degradation tag will experience fast

degradation by ClpXP leading to a low basal production rate of QS agent (α_q), whereas LuxI with a weak degradation tag will have a higher steady-state level and therefore a higher basal procution rate α_q. In contrast, once the positive feedback has been activated, the concentration of LuxI (and consequently the parameter α_q^* of the model) have a much weaker dependence on its degradataion tag since an abundance of LuxI produced from a fully activated promoter saturates the limited enzymatic processing capacity of ClpXP and therefore the level of LuxI will be determined mainly by dilution due to cell growth. As seen from equation $B.3$, decreasing α_q by a larger factor than α_q^* generally brings the system closer to oscillations, which is consistent with the requirement of a strong degradation tag for sustained oscillations demonstrated in Figure 4.2.

Microfluidic traps and multiple strains

A microfluidic trap is clearly a finite environment, but because nutrients are constantly replenished by diffusion from fresh media in the channel, logistic growth (as is often assumed in other scenarios with finite carrying capacities) would be an unrealistic description of the population dynamics. Instead, we assume that growth is unaffected as long as the population density is below the carrying capacity c of the trap. We then cap the cell density at c, corresponding to any extra cells being washed away by the flow in the main channel ("spillover"). Numerically, we reset the cell density to c after every time step of the simulation if it exceeds c. In all our simulations $c = 1$. Figure 1 shows that the system with standard parameters lyses just before it reaches the carrying capacity of the trap, so it is truly self-limiting.

For simulations of multiple strains, we simulate two copies of the system equation $B.1$ with variables $\{n_1, q_1\}$ and $\{n_2, q_2\}$. Again, we let the system evolve freely as long as $n_1 + n_2 < c$. If $n_1 + n_2$ exceeds c after any time step, we set n_1 and n_2 according

to

$$n_1 = \frac{n_1'}{n_1' + n_2'} c \qquad n_1 = \frac{n_2'}{n_1' + n_2'} c \qquad \text{if } n_1' + n_2' > c, \tag{B.4}$$

where n_1' and n_2' correspond to the population densities before the reset. More specifically, this way of limiting the total population density to the carrying capacity c corresponds to assuming a well-mixed environment, such that the relative population densities of the two strains remain unchanged upon spillover.

Consequently, two oscillating strains in one trap that use completely orthogonal quorum sensing systems only interact if the total population density hits the carrying capacity c. As shown in the main text, the strains will eventually lock into an anti-phase pattern where they avoid reaching their peak density at the same time. In order to model cross-talk, we modify the equation of the "receiver" strain (strain 2 in this case) to read

$$\frac{\mathrm{d}n_2}{\mathrm{d}t} = \alpha_2 n_2 - f(q_2 + \xi q_1)\gamma_2 n_2 \tag{B.5a}$$

$$\frac{\mathrm{d}q_2}{\mathrm{d}t} = [\alpha_{q,2} + \alpha_{q,2}^* f(q_2 + \xi q_1)]n_2 - \gamma_{q,2} q_2 \tag{B.5b}$$

where ξ determines how much strain 2 responds to the QS agent of strain 1, i.e. the strength of the cross-talk.

Appendix C

Plasmid Tables

Table C.1: Promoter Sequences Used in Chapter 2. Palindromic lux-box-like receptor-binding sequences in boldface when known.

Name	Sequence	Organism	Reference
Plux	ACTATTGTATCGCTGGGAATACAATTACTTAACATAA GC**ACCTGTAGGATCGTACAGGT**TTACGCAAGAAAA TGGTTTGTTATAGTCGAATAT	Aliivibrio fischeri	(Hasty Lab)
Ptra (pCF370)	CT**ACGTGCAGATCTGCACAT**AGCCACACCCTGAAT GAGATGTTTTCTCTCCGCTA	Agrobacterium tumefaciens	White 2007, Fuqua 1996
Plas	TTCGAGCCTAGCAAGGGTCCGGGTTCACCGAA**ATC TATCTCATTTGCTAGTT**ATAAAATTATGAAATTTGCG TAAATTCTTCA	Pseudomonas aeruginosa	(Hasty Lab)
Prpa	**ACCTGTCCGATCGGACAGTA**GTTAGGTTCCCGTTC GCACCTGCACTGTTCCCGCCTGCA	Rhodopseudomonas palustris	Hirakawa 2011
Pahy	ACCGAAGTGAAATGTTCGAGGTACTCAAGCAGTTG GTCTTGTTTCATATGCTAGCCC**CCCTGGCCAGGG**C CTCGATTATA	Aeromonas hydrophila	Garde 2010
Psma	ATAATCTTGTCATGGGTTTTAAATTTACTTGTCACAT AGGCTCTGATACAATTACTCGCCG	Serratia marcescens	Slater 2003
Prhl (qsc*rhlA*)	**TCCTGTGAAATCTGGCAGTT**ACCGTTAGCTTTCGAA TTGGCTAAAAAGTGTTC	Pseudomonas aeruginosa	Karig 2005
Pcer (PopgG)	GCTGGACGATGCGAATCTTGGAATTGCGCTCTGCA AGCCATTGAAAAACGGACGTCGTCTCTCTGATATGC CCGCTCCTGCCGCCCCCTCCGCCCGCCTGAACCG GCGCCTGCTGCTCAGCGCGGCAAGTTCGTCGCTCG CCCTCGCTGCAAGCGGGCTC	Rhodobacter sphaeroides	Puskas 1997
Pexp (PwgeA)	TGCCTGCATTT**CCGTCAGAATTACTCCTAAAATTAT ATTGTACCA**ATATTGGCACAGCATGGAGATATGTTT CGGGCACCCTCTTTCTATCAAAATATCGCCGTTTTA TTTTATGCATCTGTGTTGCGTTCGTAATTATTGCAGT GCACACTCCGGCACG	Sinorhizobium meliloti	Charoenpanich 2013
Ptra*	GC**ACGTGCAGATCTGCACAT**TTACGCAAGAAAATG GTTTGTTATAGTCGAATAT	Synthetic	This Study
Prpa*	GC**ACCTGTCCGATCGGACAGT**ATTACGCAAGAAAA TGGTTTGTTATAGTCGAATAT	Synthetic	This Study

Table C.2: Plasmids Used in Chapter 2. All constructs were expressed in E. coli DIAL Strain "EK" cells.

Plasmid	Genotype	Vector
Bsrs079-LuxR	R6K; Spec; 5' Insulation Unit; BCD7; LuxR-GFP; 3' Insulation Unit	pBjk2807
Bsrs079-LasR	R6K; Spec; 5' Insulation Unit; BCD7; LasR-GFP; 3' Insulation Unit	pBjk2807
Bsrs079-TraR	R6K; Spec; 5' Insulation Unit; BCD7; TraR-GFP; 3' Insulation Unit	pBjk2807
Bsrs079-RpaR	R6K; Spec; 5' Insulation Unit; BCD7; RpaR-GFP; 3' Insulation Unit	pBjk2807
Bsrs079-RhlR	R6K; Spec; 5' Insulation Unit; BCD7; RhlR-GFP; 3' Insulation Unit	pBjk2807
Bsrs079-SinR	R6K; Spec; 5' Insulation Unit; BCD7; SinR-GFP; 3' Insulation Unit	pBjk2807
Bsrs079-CerR	R6K; Spec; 5' Insulation Unit; BCD7; CerR-GFP; 3' Insulation Unit	pBjk2807
Bsrs079-SmaR	R6K; Spec; 5' Insulation Unit; BCD7; SmaR-GFP; 3' Insulation Unit	pBjk2807
Bsrs079-AhyR	R6K; Spec; 5' Insulation Unit; BCD7; AhyR-GFP; 3' Insulation Unit	pBjk2807
Bsrs078-LuxR	R6K; Spec; 5' Insulation Unit; BCD7; LuxR; 3' Insulation Unit	pBjk2807
Bsrs078-TraR	R6K; Spec; 5' Insulation Unit; BCD7; TraR; 3' Insulation Unit	pBjk2807
Bsrs078-TraR(W)	R6K; Spec; 5' Insulation Unit; BCD7; TraR(W); 3' Insulation Unit	pBjk2807
Bsrs078-LasR	R6K; Spec; 5' Insulation Unit; BCD7; LasR; 3' Insulation Unit	pBjk2807
Bsrs078-RpaR	R6K; Spec; 5' Insulation Unit; BCD7; RpaR; 3' Insulation Unit	pBjk2807
Bsrs074-Plux	ColE2; AmpR; Plux; u6; sfGFP	pBjk2992
Bsrs074-Ptra	ColE2; AmpR; Ptra; u6; sfGFP	pBjk2992
Bsrs074-Ptra*	ColE2; AmpR; Ptra*; u6; sfGFP	pBjk2992
Bsrs074-Plas	ColE2; AmpR; Plas; u6; sfGFP	pBjk2992
Bsrs074-Prpa	ColE2; AmpR; Prpa; u6; sfGFP	pBjk2992
Bsrs074-Prpa*	ColE2; AmpR; Prpa*; u6; sfGFP	pBjk2992
Bsrs074-Pahy	ColE2; AmpR; Pahy; u6; sfGFP	pBjk2992
Bsrs074-Psma	ColE2; AmpR; Psma; u6; sfGFP	pBjk2992
Bsrs074-Prhl	ColE2; AmpR; Prhl; u6; sfGFP	pBjk2992
Bsrs074-Pcer	ColE2; AmpR; Pcer; u6; sfGFP	pBjk2992
Bsrs074-Pexp	ColE2; AmpR; Pexp; u6; sfGFP	pBjk2992
Bsrs074-Plux-mKate2	ColE2; Cm; Plux; u6; mKate2	pBjk2992
Bsrs074-Plas-mKate2	ColE2; Cm; Plux; u6; mKate2	pBjk2992
pZA35-Bsrs074-Plux-tra	P15A; Cm; Ptra; u6; sfGFP	pZA35
Bsrs112-TraR-RpaR	R6K; Spec; 5' Insulation Unit; BCD7; TraR(W); mevB-rbs; RpaR; 3' Insulation Unit	pBjk2807
Bsrs112-TraR-LasR	R6K; Spec; 5' Insulation Unit; BCD7; TraR(W); mevB-rbs; LasR; 3' Insulation Unit	pBjk2807
Bsrs103-RpaR-RpaI	ColE1; Kan; RpaR; PluxI; RpaI; T1	pTD103
Bsrs103-RpaR-LasI	ColE1; Kan; RpaR; PluxI; LasI; T1	pTD103

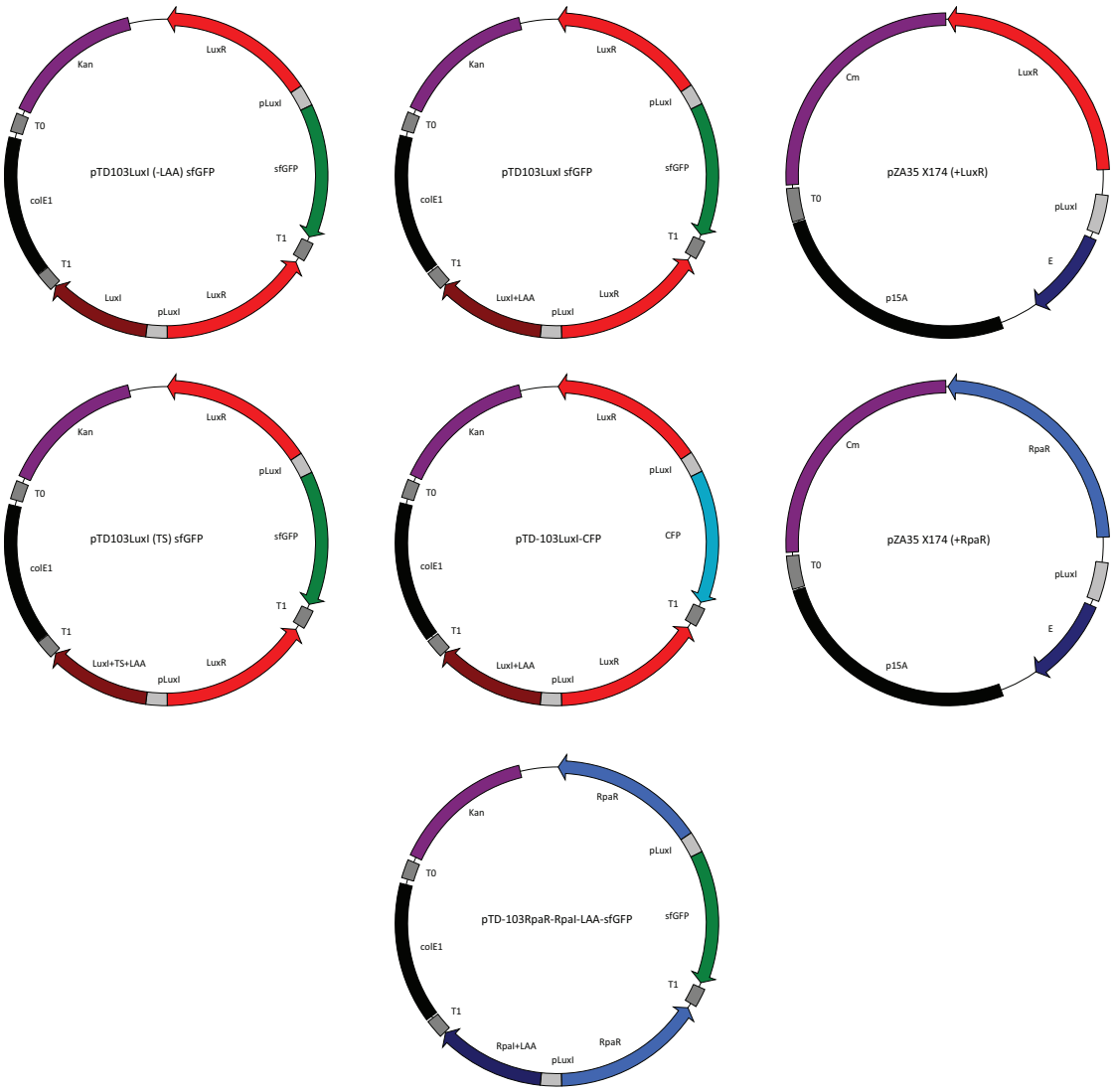

Figure C.1: Plasmid Maps Used in Chapter 4.

Table C.3: Strains Used in Chapter 4. All constructs were expressed in attenuated Salmonella SL1344.

Strain #	Strain Name	Host Bacterium	Plasmid(s)
1	MOD47	SL1344	pTD103luxI(-LAA)sfGFP + pZA35 X174E (+LuxR)
2	MOD46a	SL1344	pTD103luxI sfGFP + pZA35 X174E (+LuxR)
3	MOD46b	SL1344	pTD103luxI(TS) sfGFP + pZA35 X174E (+LuxR)
4	SRS732	SL1344	pTD103-LuxI-CFP
5	SRS800	SL1344	pTD103-LuxI-CFP + pZA35-X174E (+LuxR)
6	SRS840	SL1344	pTD103-RpaR-RPaI-LAA-sfGFP
7	SRS841	SL1344	pTD103-RpaR-RPaI-LAA-sfGFP + pZA35-X174E (+RpaR)

Bibliography

Anderson, J. C., Clarke, E. J., Arkin, A. P., and Voigt, C. A., 2006: Environmentally controlled invasion of cancer cells by engineered bacteria. *Journal of molecular biology*, **355**(4), 619–627.

Arai, T., Matsuoka, S., Cho, H.-Y., Yukawa, H., Inui, M., Wong, S.-L., and Doi, R. H., 2007: Synthesis of clostridium cellulovorans minicellulosomes by intercellular complementation. *Proceedings of the National Academy of Sciences*, **104**(5), 1456–1460.

Balagaddé, F. K., Song, H., Ozaki, J., Collins, C. H., Barnet, M., Arnold, F. H., Quake, S. R., and You, L., 2008: A synthetic escherichia coli predator–prey ecosystem. *Molecular systems biology*, **4**(1), 187.

Barbirato, F., Grivet, J. P., Soucaille, P., and Bories, A., 1996: 3-hydroxypropionaldehyde, an inhibitory metabolite of glycerol fermentation to 1, 3-propanediol by enterobacterial species. *Applied and Environmental Microbiology*, **62**(4), 1448–1451.

Basu, S., Gerchman, Y., Collins, C. H., Arnold, F. H., and Weiss, R., 2005: A synthetic multicellular system for programmed pattern formation. *Nature*, **434**(7037), 1130–1134.

Bernstein, H. C., Paulson, S. D., and Carlson, R. P., 2012: Synthetic escherichia coli consortia engineered for syntrophy demonstrate enhanced biomass productivity. *Journal of biotechnology*, **157**(1), 159–166.

Brenner, K., and Arnold, F. H., 2011: Self-organization, layered structure, and aggregation enhance persistence of a synthetic biofilm consortium. *PloS one*, **6**(2), e16791–e16791.

Brenner, K., Karig, D. K., Weiss, R., and Arnold, F. H., 2007: Engineered bidirectional communication mediates a consensus in a microbial biofilm consortium. *Proceedings of the National Academy of Sciences*, **104**(44), 17300–17304.

Brenner, K., You, L., and Arnold, F. H., 2008: Engineering microbial consortia: a new frontier in synthetic biology. *Trends in biotechnology*, **26**(9), 483–489.

Brockman, I. M., and Prather, K. L., 2015: Dynamic metabolic engineering: New strategies for developing responsive cell factories. *Biotechnology journal*.

Brophy, J. A., and Voigt, C. A., 2014: Principles of genetic circuit design. *Nature methods*, **11**(5), 508–520.

Burmolle, M., Webb, J. S., Rao, D., Hansen, L. H., Sorensen, S. J., and Kjelleberg, S., 2006: Enhanced biofilm formation and increased resistance to antimicrobial agents and bacterial invasion are caused by synergistic interactions in multispecies biofilms. *Applied and environmental microbiology*, **72**(6), 3916–3923.

Canton, B., Labno, A., and Endy, D., 2008: Refinement and standardization of synthetic biological parts and devices. *Nature biotechnology*, **26**(7), 787–793.

Carlson, R. P., and Taffs, R. L., 2010: Molecular-level tradeoffs and metabolic adaptation to simultaneous stressors. *Current opinion in biotechnology*, **21**(5), 670–676.

Charoenpanich, P., Meyer, S., Becker, A., and McIntosh, M., 2013: Temporal expression program of quorum sensing-based transcription regulation in sinorhizobium meliloti. *Journal of bacteriology*, **195**(14), 3224–3236.

Chen, Y., 2011: Development and application of co-culture for ethanol production by co-fermentation of glucose and xylose: a systematic review. *Journal of industrial microbiology & biotechnology*, **38**(5), 581–597.

Chickarmane, V., Kholodenko, B. N., and Sauro, H. M., 2007: Oscillatory dynamics arising from competitive inhibition and multisite phosphorylation. *Journal of Theoretical Biology*, **244**(1), 68–76.

Chuang, J. S., 2012: Engineering multicellular traits in synthetic microbial populations. *Current opinion in chemical biology*, **16**(3), 370–378.

Danino, T., Mondragón-Palomino, O., Tsimring, L., and Hasty, J., 2010: A synchronized quorum of genetic clocks. *Nature*, **463**(7279), 326–330.

Davis, R. M., Muller, R. Y., and Haynes, K. A., 2015: Can the natural diversity of quorum-sensing advance synthetic biology? *Frontiers in bioengineering and biotechnology*, **3**.

De Roy, K., Marzorati, M., Negroni, A., Thas, O., Balloi, A., Fava, F., Verstraete, W., Daffonchio, D., and Boon, N., 2013: Environmental conditions and community evenness determine the outcome of biological invasion. *Nature communications*, **4**, 1383.

De Roy, K., Marzorati, M., Van den Abbeele, P., Van de Wiele, T., and Boon, N., 2014: Synthetic microbial ecosystems: an exciting tool to understand and apply microbial communities. *Environmental microbiology*, **16**(6), 1472–1481.

Dejonghe, W., Berteloot, E., Goris, J., Boon, N., Crul, K., Maertens, S., Höfte, M., De Vos, P., Verstraete, W., and Top, E. M., 2003: Synergistic degradation of linuron by a bacterial consortium and isolation of a single linuron-degrading variovorax strain. *Applied and Environmental Microbiology*, **69**(3), 1532–1541.

Din, M. O., Danino, T., Prindle, A., Skalak, M., Selimkhanov, J., Allen, K., Julio, E., Atolia, E., Tsimring, L. S., Bhatia, S. N., et al., 2016: Synchronized cycles of bacterial lysis for in vivo delivery. *Nature*, **536**(7614), 81–85.

Dueber, J. E., Wu, G. C., Malmirchegini, G. R., Moon, T. S., Petzold, C. J., Ullal, A. V., Prather, K. L., and Keasling, J. D., 2009: Synthetic protein scaffolds provide modular control over metabolic flux. *Nature biotechnology*, **27**(8), 753–759.

Dunham, M. J., 2007: Synthetic ecology: a model system for cooperation. *Proceedings of the National Academy of Sciences*, **104**(6), 1741–1742.

Eiteman, M. A., Lee, S. A., and Altman, E., 2008: A co-fermentation strategy to consume sugar mixtures effectively. *J Biol Eng*, **2**(3).

Elowitz, M. B., and Leibler, S., 2000: A synthetic oscillatory network of transcriptional regulators. *Nature*, **403**(6767), 335–338.

Endy, D., 2005: Foundations for engineering biology. *Nature*, **438**(7067), 449–453.

Faust, K., and Raes, J., 2012: Microbial interactions: from networks to models. *Nature Reviews Microbiology*, **10**(8), 538–550.

Fay, P., 1992: Oxygen relations of nitrogen fixation in cyanobacteria. *Microbiological reviews*, **56**(2), 340.

Ford, T. J., and Silver, P. A., 2015: Synthetic biology expands chemical control of microorganisms. *Current opinion in chemical biology*, **28**, 20–28.

Foster, K. R., and Bell, T., 2012: Competition, not cooperation, dominates interactions among culturable microbial species. *Current biology*, **22**(19), 1845–1850.

Freilich, S., Zarecki, R., Eilam, O., Segal, E. S., Henry, C. S., Kupiec, M., Gophna, U., Sharan, R., and Ruppin, E., 2011: Competitive and cooperative metabolic interactions in bacterial communities. *Nature communications*, **2**, 589.

Fulget, N., Poughon, L., Richalet, J., and Lasseur, C., 1999: Melissa: global control strategy of the artificial ecosystem by using first principles models of the compartments. *Advances in Space Research*, **24**(3), 397–405.

Fuqua, C., and Greenberg, E. P., 2002: Listening in on bacteria: acyl-homoserine lactone signalling. *Nature Reviews Molecular Cell Biology*, **3**(9), 685–695.

Fuqua, C., and Winans, S. C., 1996: Conserved cis-acting promoter elements are required for density-dependent transcription of agrobacterium tumefaciens conjugal transfer genes. *Journal of Bacteriology*, **178**(2), 435–440.

Fuqua, C., Winans, S. C., and Greenberg, E. P., 1996: Census and consensus in bacterial ecosystems: the luxr-luxi family of quorum-sensing transcriptional regulators. *Annual Reviews in Microbiology*, **50**(1), 727–751.

Garde, C., Bjarnsholt, T., Givskov, M., Jakobsen, T. H., Hentzer, M., Claussen, A., Sneppen, K., Ferkinghoff-Borg, J., and Sams, T., 2010: Quorum sensing regulation in aeromonas hydrophila. *Journal of molecular biology*, **396**(4), 849–857.

Gardner, T. S., Cantor, C. R., and Collins, J. J., 2000: Construction of a genetic toggle switch in escherichia coli. *Nature*, **403**(6767), 339–342.

Gause, G. F., 2003: *The struggle for existence*. Courier Corporation.

Gravel, D., Bell, T., Barbera, C., Bouvier, T., Pommier, T., Venail, P., and Mouquet, N., 2011: Experimental niche evolution alters the strength of the diversity-productivity relationship. *Nature*, **469**(7328), 89–92.

Gray, K. M., and Garey, J. R., 2001: The evolution of bacterial luxi and luxr quorum sensing regulators. *Microbiology*, **147**(8), 2379–2387.

Großkopf, T., and Soyer, O. S., 2014: Synthetic microbial communities. *Current opinion in microbiology*, **18**, 72–77.

Hillesland, K. L., and Stahl, D. A., 2010: Rapid evolution of stability and productivity at the origin of a microbial mutualism. *Proceedings of the National Academy of Sciences*, **107**(5), 2124–2129.

Hirakawa, H., Oda, Y., Phattarasukol, S., Armour, C. D., Castle, J. C., Raymond, C. K., Lappala, C. R., Schaefer, A. L., Harwood, C. S., and Greenberg, E. P., 2011: Activity of the rhodopseudomonas palustris p-coumaroyl-homoserine lactone-responsive transcription factor rpar. *Journal of bacteriology*, **193**(10), 2598–2607.

Hong, S. H., Hegde, M., Kim, J., Wang, X., Jayaraman, A., and Wood, T. K., 2012: Synthetic quorum-sensing circuit to control consortial biofilm formation and dispersal in a microfluidic device. *Nature communications*, **3**, 613.

Huang, S., and Pang, L., 2012: Comparing statistical methods for quantifying drug sensitivity based on in vitro dose–response assays. *Assay and drug development technologies*, **10**(1), 88–96.

Karig, D., and Weiss, R., 2005: Signal-amplifying genetic circuit enables in vivo observation of weak promoter activation in the rhl quorum sensing system. *Biotechnology and bioengineering*, **89**(6), 709–718.

Kerner, A., Park, J., Williams, A., and Lin, X. N., 2012: A programmable escherichia coli consortium via tunable symbiosis. *PLoS One*, **7**(3), e34032.

Kerr, B., Riley, M. A., Feldman, M. W., and Bohannan, B. J., 2002: Local dispersal promotes biodiversity in a real-life game of rock–paper–scissors. *Nature*, **418**(6894), 171–174.

Khalil, A. S., and Collins, J. J., 2010: Synthetic biology: applications come of age. *Nature Reviews Genetics*, **11**(5), 367–379.

Khoruts, A., Dicksved, J., Jansson, J. K., and Sadowsky, M. J., 2010: Changes in the composition of the human fecal microbiome after bacteriotherapy for recurrent clostridium difficile-associated diarrhea. *Journal of clinical gastroenterology*, **44**(5), 354–360.

Kittleson, J. T., Cheung, S., and Anderson, J. C., 2011: Rapid optimization of gene dosage in e. coli using dial strains. *J Biol Eng*, **5**(10).

Kizer, L., Pitera, D. J., Pfleger, B. F., and Keasling, J. D., 2008: Application of functional genomics to pathway optimization for increased isoprenoid production. *Applied and environmental microbiology*, **74**(10), 3229–3241.

Klitgord, N., and Segre, D., 2010: Environments that induce synthetic microbial ecosystems. *PLoS Comput Biol*, **6**(11), e1001002.

Kneitel, J. M., and Chase, J. M., 2004: Trade-offs in community ecology: linking spatial scales and species coexistence. *Ecology Letters*, **7**(1), 69–80.

Kobayashi, H., Kærn, M., Araki, M., Chung, K., Gardner, T. S., Cantor, C. R., and Collins, J. J., 2004: Programmable cells: interfacing natural and engineered gene networks. *Proceedings of the National Academy of Sciences of the United States of America*, **101**(22), 8414–8419.

LaPara, T., Zakharova, T., Nakatsu, C., and Konopka, A., 2002: Functional and structural adaptations of bacterial communities growing on particulate substrates under stringent nutrient limitation. *Microbial ecology*, **44**(4), 317–326.

Lutz, R., and Bujard, H., 1997: Independent and tight regulation of transcriptional units in escherichia coli via the lacr/o, the tetr/o and arac/i1-i2 regulatory elements. *Nucleic acids research*, **25**(6), 1203–1210.

Marchand, N., and Collins, C. H., 2013: Peptide-based communication system enables escherichia coli to bacillus megaterium interspecies signaling. *Biotechnology and bioengineering*, **110**(11), 3003–3012.

Marguet, P., Tanouchi, Y., Spitz, E., Smith, C., and You, L., 2010: Oscillations by minimal bacterial suicide circuits reveal hidden facets of host-circuit physiology. *PloS one*, **5**(7), e11909.

Mather, W., Mondragón-Palomino, O., Danino, T., Hasty, J., and Tsimring, L. S., 2010: Streaming instability in growing cell populations. *Physical review letters*, **104**(20), 208101.

McDaniel, R., and Weiss, R., 2005: Advances in synthetic biology: on the path from prototypes to applications. *Current Opinion in Biotechnology*, **16**(4), 476–483.

McMahon, K. D., Martin, H. G., and Hugenholtz, P., 2007: Integrating ecology into biotechnology. *Current opinion in biotechnology*, **18**(3), 287–292.

Mee, M. T., Collins, J. J., Church, G. M., and Wang, H. H., 2014: Syntrophic exchange in synthetic microbial communities. *Proceedings of the National Academy of Sciences*, **111**(20), E2149–E2156.

Miller, M. B., and Bassler, B. L., 2001: Quorum sensing in bacteria. *Annual Reviews in Microbiology*, **55**(1), 165–199.

Minty, J. J., Singer, M. E., Scholz, S. A., Bae, C.-H., Ahn, J.-H., Foster, C. E., Liao, J. C., and Lin, X. N., 2013: Design and characterization of synthetic fungal-bacterial consortia for direct production of isobutanol from cellulosic biomass. *Proceedings of the National Academy of Sciences*, **110**(36), 14592–14597.

Mutalik, V. K., Guimaraes, J. C., Cambray, G., Lam, C., Christoffersen, M. J., Mai, Q.-A., Tran, A. B., Paull, M., Keasling, J. D., Arkin, A. P., and Endy, D., 2013a: Precise and reliable gene expression via standard transcription and translation initiation elements. *Nature methods*, **10**(4), 354–360.

Mutalik, V. K., Guimaraes, J. C., Cambray, G., Mai, Q.-A., Christoffersen, M. J., Martin, L., Yu, A., Lam, C., Rodriguez, C., and Bennett, G., 2013b: Quantitative estimation of activity and quality for collections of functional genetic elements. *Nature methods*, **10**(4), 347–353.

Ng, W.-L., and Bassler, B. L., 2009: Bacterial quorum-sensing network architectures. *Annual review of genetics*, **43**, 197.

Paddon, C. J., Westfall, P. J., Pitera, D., Benjamin, K., Fisher, K., McPhee, D., Leavell, M., Tai, A., Main, A., Eng, D., et al., 2013: High-level semi-synthetic production of the potent antimalarial artemisinin. *Nature*, **496**(7446), 528–532.

Pai, A., Tanouchi, Y., and You, L., 2012: Optimality and robustness in quorum sensing (qs)-mediated regulation of a costly public good enzyme. *Proceedings of the National Academy of Sciences*, **109**(48), 19810–19815.

Pandhal, J., and Noirel, J., 2014: Synthetic microbial ecosystems for biotechnology. *Biotechnology letters*, **36**(6), 1141–1151.

Patle, S., and Lal, B., 2007: Ethanol production from hydrolysed agricultural wastes using mixed culture of zymomonas mobilis and candida tropicalis. *Biotechnology letters*, **29**(12), 1839–1843.

Payne, S., Li, B., Cao, Y., Schaeffer, D., Ryser, M. D., and You, L., 2013: Temporal control of self-organized pattern formation without morphogen gradients in bacteria. *Molecular systems biology*, **9**(1), 697.

Pédelacq, J.-D., Cabantous, S., Tran, T., Terwilliger, T. C., and Waldo, G. S., 2006: Engineering and characterization of a superfolder green fluorescent protein. *Nature biotechnology*, **24**(1), 79–88.

Petrof, E. O., Gloor, G. B., Vanner, S. J., Weese, S. J., Carter, D., Daigneault, M. C., Brown, E. M., Schroeter, K., and Allen-Vercoe, E., 2013: Stool substitute transplant therapy for the eradication of clostridium difficile infection:?repoopulating?the gut. *Microbiome*, **1**(1), 1.

Prindle, A., Samayoa, P., Razinkov, I., Danino, T., Tsimring, L. S., and Hasty, J., 2012: A sensing array of radically coupled genetic/biopixels/'. *Nature*, **481**(7379), 39–44.

Prindle, A., Selimkhanov, J., Li, H., Razinkov, I., Tsimring, L. S., and Hasty, J., 2014: Rapid and tunable post-translational coupling of genetic circuits. *Nature*, **508**(7496), 387–391.

Purnick, P. E., and Weiss, R., 2009: The second wave of synthetic biology: from modules to systems. *Nature reviews Molecular cell biology*, **10**(6), 410–422.

Puskas, A., Greenberg, E. á., Kaplan, S., and Schaefer, A. á., 1997: A quorum-sensing system in the free-living photosynthetic bacterium rhodobacter sphaeroides. *Journal of bacteriology*, **179**(23), 7530–7537.

Quan, D. N., Tsao, C.-Y., Wu, H.-C., and Bentley, W. E., 2016: Quorum sensing desynchronization leads to bimodality and patterned behaviors. *PLOS Comput Biol*, **12**(4), e1004781.

Quan, J., and Tian, J., 2009: Circular polymerase extension cloning of complex gene libraries and pathways. *PloS one*, **4**(7), e6441.

Ro, D.-K., Paradise, E. M., Ouellet, M., Fisher, K. J., Newman, K. L., Ndungu, J. M., Ho, K. A., Eachus, R. A., Ham, T. S., Kirby, J., and Keasling, J. D., 2006: Production of the antimalarial drug precursor artemisinic acid in engineered yeast. *Nature*, **440**(7086), 940–943.

Saeidi, N., Wong, C. K., Lo, T.-M., Nguyen, H. X., Ling, H., Leong, S. S. J., Poh, C. L., and Chang, M. W., 2011: Engineering microbes to sense and eradicate pseudomonas aeruginosa, a human pathogen. *Molecular systems biology*, **7**(1), 521.

Schaefer, A. L., Greenberg, E., Oliver, C. M., Oda, Y., Huang, J. J., Bittan-Banin, G., Peres, C. M., Schmidt, S., Juhaszova, K., and Sufrin, J. R., 2008: A new class of homoserine lactone quorum-sensing signals. *Nature*, **454**(7204), 595–599.

Scott, S. R., and Hasty, J., 2016: Quorum sensing communication modules for microbial consortia. *ACS synthetic biology*.

Shahinas, D., Silverman, M., Sittler, T., Chiu, C., Kim, P., Allen-Vercoe, E., Weese, S., Wong, A., Low, D. E., and Pillai, D. R., 2012: Toward an understanding of changes in diversity associated with fecal microbiome transplantation based on 16s rrna gene deep sequencing. *MBio*, **3**(5), e00338–12.

Shong, J., and Collins, C. H., 2013: Engineering the esar promoter for tunable quorum sensing-dependent gene expression. *ACS synthetic biology*, **2**(10), 568–575.

Shou, W., Ram, S., and Vilar, J. M., 2007: Synthetic cooperation in engineered yeast populations. *Proceedings of the National Academy of Sciences*, **104**(6), 1877–1882.

Slater, H., Crow, M., Everson, L., and Salmond, G. P., 2003: Phosphate availability regulates biosynthesis of two antibiotics, prodigiosin and carbapenem, in serratia via both quorum-sensing-dependent and-independent pathways. *Molecular microbiology*, **47**(2), 303–320.

Srimani, J. K., and You, L., 2014: Emergent dynamics from quorum eavesdropping. *Chemistry & biology*, **21**(12), 1601–1602.

Steen, E. J., Kang, Y., Bokinsky, G., Hu, Z., Schirmer, A., McClure, A., Del Cardayre, S. B., and Keasling, J. D., 2010: Microbial production of fatty-acid-derived fuels and chemicals from plant biomass. *Nature*, **463**(7280), 559–562.

Stricker, J., Cookson, S., Bennett, M. R., Mather, W. H., Tsimring, L. S., and Hasty, J., 2008: A fast, robust and tunable synthetic gene oscillator. *Nature*, **456**(7221), 516–519.

Summers, Z. M., Fogarty, H. E., Leang, C., Franks, A. E., Malvankar, N. S., and Lovley, D. R., 2010: Direct exchange of electrons within aggregates of an evolved syntrophic coculture of anaerobic bacteria. *Science*, **330**(6009), 1413–1415.

Swift, S., Karlyshev, A. V., Fish, L., Durant, E. L., Winson, M. K., Chhabra, S. R., Williams, P., Macintyre, S., and Stewart, G., 1997: Quorum sensing in aeromonas hydrophila and aeromonas salmonicida: identification of the luxri homologs ahyri and asari and their cognate n-acylhomoserine lactone signal molecules. *Journal of bacteriology*, **179**(17), 5271–5281.

Tabor, J. J., Salis, H. M., Simpson, Z. B., Chevalier, A. A., Levskaya, A., Marcotte, E. M., Voigt, C. A., and Ellington, A. D., 2009: A synthetic genetic edge detection program. *Cell*, **137**(7), 1272–1281.

Tamsir, A., Tabor, J. J., and Voigt, C. A., 2011: Robust multicellular computing using genetically encoded nor gates and chemical/wires/'. *Nature*, **469**(7329), 212–215.

Tanouchi, Y., Smith, R. P., and You, L., 2012: Engineering microbial systems to explore ecological and evolutionary dynamics. *Current opinion in biotechnology*, **23**(5), 791–797.

Thomson, N., Crow, M., McGowan, S., Cox, A., and Salmond, G., 2000: Biosynthesis of carbapenem antibiotic and prodigiosin pigment in serratia is under quorum sensing control. *Molecular microbiology*, **36**(3), 539–556.

Tsao, C.-Y., Hooshangi, S., Wu, H.-C., Valdes, J. J., and Bentley, W. E., 2010: Autonomous induction of recombinant proteins by minimally rewiring native quorum sensing regulon of e. coli. *Metabolic engineering*, **12**(3), 291–297.

Vannini, A., Volpari, C., Gargioli, C., Muraglia, E., Cortese, R., De Francesco, R., Neddermann, P., and Di Marco, S., 2002: The crystal structure of the quorum sensing protein trar bound to its autoinducer and target dna. *The EMBO journal*, **21**(17), 4393–4401.

Vinuselvi, P., and Lee, S. K., 2012: Engineered escherichia coli capable of co-utilization of cellobiose and xylose. *Enzyme and microbial technology*, **50**(1), 1–4.

Voigt, C. A., 2006: Genetic parts to program bacteria. *Current opinion in biotechnology*, **17**(5), 548–557.

Volfson, D., Cookson, S., Hasty, J., and Tsimring, L. S., 2008: Biomechanical ordering of dense cell populations. *Proceedings of the National Academy of Sciences*, **105**(40), 15346–15351.

Waters, C. M., and Bassler, B. L., 2005: Quorum sensing: cell-to-cell communication in bacteria. *Annu. Rev. Cell Dev. Biol.*, **21**, 319–346.

West, S. A., Griffin, A. S., Gardner, A., and Diggle, S. P., 2006: Social evolution theory for microorganisms. *Nature Reviews Microbiology*, **4**(8), 597–607.

White, C. E., and Winans, S. C., 2007: The quorum-sensing transcription factor trar decodes its dna binding site by direct contacts with dna bases and by detection of dna flexibility. *Molecular microbiology*, **64**(1), 245–256.

Wintermute, E. H., and Silver, P. A., 2010: Emergent cooperation in microbial metabolism. *Molecular systems biology*, **6**(1), 407.

Wu, F., Menn, D. J., and Wang, X., 2014: Quorum-sensing crosstalk-driven synthetic circuits: From unimodality to trimodality. *Chemistry & biology*, **21**(12), 1629–1638.

Yadav, B., Pemovska, T., Szwajda, A., Kulesskiy, E., Kontro, M., Karjalainen, R., Majumder, M. M., Malani, D., Murumägi, A., and Knowles, J., 2014: Quantitative scoring of differential drug sensitivity for individually optimized anticancer therapies. *Scientific reports*, **4**.

You, L., Cox, R. S., Weiss, R., and Arnold, F. H., 2004: Programmed population control by cell–cell communication and regulated killing. *Nature*, **428**(6985), 868–871.

Zemke, A. C., and Bomberger, J. M., 2016: Microbiology: Social suicide for a good cause. *Current Biology*, **26**(2), R80–R82.

Zhou, K., Qiao, K., Edgar, S., and Stephanopoulos, G., 2015: Distributing a metabolic pathway among a microbial consortium enhances production of natural products. *Nature biotechnology*, **33**(4), 377–383.

Zhu, J., and Winans, S. C., 1999: Autoinducer binding by the quorum-sensing regulator trar increases affinity for target promoters in vitro and decreases trar turnover rates in whole cells. *Proceedings of the National Academy of Sciences*, **96**(9), 4832–4837.

Zhu, M. M., Lawman, P. D., and Cameron, D. C., 2002: Improving 1, 3-propanediol production from glycerol in a metabolically engineered escherichia coliby reducing accumulation of sn-glycerol-3-phosphate. *Biotechnology progress*, **18**(4), 694–699.